NASA Technical Memorandum 78576

A Study of Redundancy Management Strategy for Tetrad Strap-Down Inertial Systems

Ronald J. Hruby, William S. Bjorkman,
Stanley F. Schmidt and Ralph A. Carestia

February 1979

NASA
National Aeronautics and
Space Administration

NOTATION

a_{ij}	pentad parity coefficients used in the pseudosensor
B	vector of constrained-fit polynomial coefficients whose elements are b_{ij}
b	subscript or superscript for "body" frame
$\tilde{b}$	sensor bias error
b_i	bias compensation for sensor i
b_{ij}	polynomial coefficient for sensor i, order j, prefailure
b'_{ij}	polynomial coefficient for sensor i, order j, postfailure
C	weighted measurement sum 3p-vector whose elements are c^j
c	subscript for "constrained-fit" solution
c^j	weighted measurement sum 3-vector of order j used in the constrained-fit formulation
c_{5i}	pseudosensor mapping coefficients, prefailure
c'_{5i}	pseudosensor mapping coefficients, postfailure
d	(1) summed parity residual detection threshold value; (2) subscript for "detection"
F	specific force
FD	data frames required to detect a failure
G	matrix of sensitivities used in the constrained fit
g	gravity
$H(\tau)$	constrained-fit sensitivity matrix corresponding to time τ
i	(1) subscript for sensor number; (2) subscript for "isolation;" (3) summation index
j	index usually used for polynomial order
k_c	index of the faulty sensor as identified by the constrained-fit strategy

k_p	index of the faulty sensor as identified by the pseudosensor strategy
M_i	mass-unbalance compensation vector for gyro i
m, $m(\tau)$	measurement 4-vector whose elements are m_1, $m_i(\tau)$ at time τ
m_i, $m_i(\tau)$	measurement from sensor i at time τ
$\hat{m}$, $\hat{m}_i$	estimated or predicted value of m, m_i
N	number of data points (frames) in the isolation interval
n	number of data points (frames) in the fit interval
P	information matrix defined for the constrained fit
p	(1) phenomenological input vector (Ω or F); (2) order of a polynomial; (3) subscript for "parity residual;" (4) subscript for "pseudosensor" solution
q	quantization in engineering units per bit in sensor output
$\tilde{q}_i$	quantization error in sensor i
$\tilde{r}_i$	random or unmodeled error in the output of sensor i
r_5	rms pseudosensor residual in the fit interval
S_i	scale factor and alignment compensation vector for sensor i
$\tilde{s}$	scale factor error
T	superscript meaning "transposed"
t	(1) time; (2) subscript or superscript for "tetrad" frame
t_a	apparent time of failure
t_d	time of failure detection
t_0	fit reference time
${}^t T^b$	transformation from body to tetrad coordinates
${}^b T^t$	transformation from tetrad to body coordinates
${}^b U$, ${}^t U$	matrices whose four columns are ${}^b u_i$ or ${}^t u_i$ for $i = 1, 2, 3, 4$
u_i	unit vector along the input axis of sensor i

$\hat{u}_i$	estimated value of u_i
${}_b u_i$, ${}_t u_i$	u_i expressed in the body (b) or tetrad (t) frame
Y	measurement residual vector used in the constrained fit formulation
α	parity coefficient corresponding to sensor No. 1
α_{k_c}, α_{k_p}	parity coefficient of the apparently failed sensor
β	parity coefficient corresponding to sensor No. 2
γ	parity coefficient corresponding to sensor No. 3
Δ	measurement sampling interval or time corresponding to one data frame
$\Delta v_i(t)$	velocity increment measured by accelerometer i at time t
$\Delta\theta_i(t)$	rotation increment measured by gyro i at time t
δ_i	measurement residual of sensor i used in the constrained-fit strategy
Σi^j	sum of integers i raised to the power j
$\Sigma(i\Delta)^j m_k(i\Delta)$	sum of weighted measurements in the constrained fit
$\Sigma\delta_i$	sum of the constrained-fit residuals for sensor i across the isolation interval
$\Sigma\delta_{max}$	sum of the apparently failed sensor's measurement residuals across the isolation interval
$\Sigma\delta_{nl}$	second largest constrained-fit residual sum
$\Sigma\epsilon_i$	sum of the pseudosensor pentad parity residuals across the isolation interval
$\Sigma\epsilon_{min}$	sum of the apparently failed sensor's parity residual across the isolation interval
$\Sigma\epsilon_{ns}$	second smallest parity residual sum in the isolation interval
ϵ_i, $\epsilon_i(\tau)$	tetrad parity residual excluding sensor i in the pseudo-pentad configuration

ε_5	parity residual which excludes the fifth (pseudo) sensor, used for detection of failures
$\bar{\varepsilon}_5$	average value of ε_5 in the isolation interval
η	angle between the skewed sensor and each mutually orthogonal sensor in the ortho-skew configuration
λ_i	threshold for confidence measure i
σ_f	rms constrained fit residual in the fit interval
σ_i	rms constrained fit residual in the isolation interval
σ_p	rms parity residual
τ	(1) time relative to the fit reference time, t_0; (2) time variable for integration; (3) generic time, as in $m(\tau)$
τ_d	time interval corresponding to the detection window
τ_f	time interval used in a polynomial fit
τ_i	time interval for isolation
Ω	angular velocity

Other Symbols:

$\{x\}$	integer part of x
$\hat{x}$	estimated or predicted value of x
$\tilde{x}$	error in estimating x

A STUDY OF A REDUNDANCY MANAGEMENT STRATEGY FOR TETRAD STRAP-DOWN INERTIAL SYSTEMS

Ronald J. Hruby, William S. Bjorkman,* Stanley F. Schmidt,* and Ralph A. Carestia**

Ames Research Center

SUMMARY

A redundancy management strategy for a tetrad strap-down inertial system is described. Algorithms are developed that attempt to identify which sensor in a tetrad configuration has experienced a step failure. An algorithm is also described that provides a measure of the confidence with which the correct identification has been made. Experimental results are presented from real-time tests conducted on a three-axis motion facility utilizing an orthoskew tetrad strap-down inertial sensor package. The effects of prediction errors and of quantization on correct failure identification are discussed as well as an algorithm for detecting second failures through prediction.

INTRODUCTION

The use of skewed, redundant, strapped-down inertial sensors is a promising, cost-effective approach for gaining improved reliability for on-board inertial sensing systems in aircraft (ref. 1). It is only recently, however, that inertial sensors with adequate long-term calibration stability for these strap-down applications have become available. For example, the ring laser gyro, whose development started in the early 1960s, is available now in prototype production and has been extensively flight tested. For "single thread" flight control, three-axis orthogonal (triad) sensing with such instruments is required. By adding one more sensor whose axis is skewed with respect to the orthogonal triad we obtain the potential for a fail-safe system in that any three of the four sensors are adequate to provide the necessary triad information. A system with four sensors will be called a "tetrad" system. To have a fail-safe (FS) capability, we need a means for detecting that a sensor has failed so that the whole system can be switched off-line. To have a fail-operational (FO) system we need a means of not only detecting that a failure has occurred, but also of isolating (i.e., identifying and removing from calculational dependence) the failed sensor before it can cause deleterious effects in the flight control system.

The primary objective of this study effort was to investigate the feasibility of identifying the failed sensor in a tetrad configured system. Previous work (see refs. 2-5) was directed at the failed sensor detection problem

---

*Analytical Mechanics Associates, Mountain View, California.
**University of Southern Colorado, Pueblo, Colorado.

for free-inertial navigation applications and did not consider the possibility of identifying the failed sensor in a tetrad configuration. The material presented in this paper includes the description of a tetrad sensor failure-detection algorithm and dual algorithms for identifying the failed sensor. A confidence algorithm whose purpose is to exclude erroneous identifications is also described. The joint application of the detection, dual identification, and confidence algorithms comprises the redundancy management strategy for a tetrad sensor system that is analyzed in this report.

The experimental evaluation was limited to step-type failures. In this type of failure, the output of the instrument jumps by some value at the time of the failure and remains biased by this value thereafter. The step-failure model was adopted because of its simplicity. The ability of the algorithms to detect and identify sensors which have undergone a step failure is a necessary, but not sufficient, condition for their application to aircraft system implementation.

The evaluation was limited to one particular tetrad configuration, the ortho-skew configuration shown in figure 1. One of the sensor axes is skewed, forming equal angles (about 54.735°) with each of the three othogonal axes. Failure detection and identification results presented in this paper are restricted to gyro failures. Accelerometer failure detection and isolation is entirely analogous to that for gyros.

TETRAD FAILURE DETECTION, IDENTIFICATION, AND CONFIDENCE ALGORITHMS

The failure-detection, identification, and confidence algorithms for the tetrad strap-down inertial sensor system must detect that a sensor failure has occurred, identify it without error, and remove it from the computational stream. The general strap-down tetrad sensor package includes four gyros and four accelerometers. The ortho-skew tetrad configuration used in this study has three mutually orthogonal sensors and one skewed sensor whose input axis is angularly equidistant from each of the mutually orthogonal sensor axes. The ensuing explains details of the redundancy management strategy used for the tetrad.

Symbol and Variable Conventions

The tetrad reference frame is orthonormal and corresponds physically to the edges of the box containing the tetrad instrument package. The orthogonal sensors' input axes are (neglecting misalignments) parallel to the axes of the tetrad reference frame. The transformation of coordinates to the tetrad frame from the current body reference frame, in which the tetrad instrument package is mounted, will be denoted ${}_{t}T^{b}$.

Let u_i represent a unit vector along the input axis direction of the ith sensor. This vector will be denoted ${}_{t}u_i$ when it is expressed in

tetrad-frame components and ${}_bu_i$ in the body frame (${}_bu_i = {}_bT^t\,{}_tu_i$). The tetrad-frame components of the four sensor axes are denoted by the 3 × 4 matrix, ${}_tU$.

$$ {}_tU = ({}_tu_1 \quad {}_tu_2 \quad {}_tu_3 \quad {}_tu_4) = \begin{pmatrix} 1 & 0 & 0 & \cos\eta \\ 0 & 1 & 0 & \cos\eta \\ 0 & 0 & 1 & \cos\eta \end{pmatrix} \tag{1} $$

The right-most equality is true only for the ortho-skew configuration. The angle η is the angle between the skewed sensor's (sensor No. 4) input axis and the axes of each of the orthogonal sensors. The body-frame components of the four sensor axes are:

$$ {}_bU = ({}_bu_1 \quad {}_bu_2 \quad {}_bu_3 \quad {}_bu_4) = {}_bT^t\,{}_tU \tag{2} $$

Any of the sensing-axis unit vectors can be written as a linear combination of the other three. In particular,

$$ u_4 = \alpha u_1 + \beta u_2 + \gamma u_3 \ . \tag{3} $$

Measurement Model

The sensors considered in this paper are of the integrating type so that the output measurement is the integral of the sensed input over the sampling time interval, Δ.

This output measurement is observed as counts where each count has the value q. In this paper, the equivalent gyro quantization q is 3.136 arc-seconds. Every measurement readout is an integer number of counts. A non-destructive readout is assumed, so that any remaining fraction of a count is not lost, but is added into the counts for the next time interval.

A gyro whose sensing axis is u_i senses the component of angular velocity Ω which lies along u_i. More generally, the gyro's measured output is a scaled version of $u_i \cdot \Omega$ which includes bias, quantization, and other effects. The gyro measurement model adopted for this paper is

$$ \Delta\theta_i(t) = \left\{ \int_{t-\Delta}^{t} (b_i + S_i \cdot \Omega + M_i \cdot F)d\tau + \tilde{q}_i + \tilde{r}_i \right\} \tag{4} $$

A similar model for accelerometer measurements is

$$ \Delta v_i(t) = \left\{ \int_{t-\Delta}^{t} (b_i + S_i \cdot F)d\tau + \tilde{q}_i + \tilde{r}_i \right\} \tag{5} $$

In these equations, the notation "{}" means "integer part of," b_i is bias, S_i is the product of u_i and the sensor's scale factor, M_i is a

vector of mass-unbalance coefficients, F is specific force, $\tilde{q}_i$ is quantization error, and $\tilde{r}_i$ is random error. The quantities b_i, S_i and M_i are estimated for each sensor by a calibration procedure described in the appendix. The gyro measurements are used to estimate Ω and accelerometer measurements are used to estimate F. The generic notation adopted for the input vector to be estimated from the sensors is p; the generic notation adopted for the ith sensor's output is m_i.

The equation

$$m_i = u_i \cdot \int p d\tau \tag{6}$$

therefore illustrates, approximately, the relationship between the input, and sensor's output, m.

Computation of Orthogonal Triad Equivalent Measurements

In order for aircraft sensor measurements to be useful in aircraft navigation or control, they must first be transformed from the tetrad reference frame into equivalent orthogonal triad measurements relative to the aircraft body reference frame. When four sensors are thought to be operational (no failures yet detected), a least-squares procedure is used to effect the transformation. From equation (6) we have

$$\begin{pmatrix} m_1 \\ m_2 \\ m_3 \\ m_4 \end{pmatrix} = {}_bU^T \; {}_b\int p d\tau \tag{7}$$

where the lower left subscript, b, means "expressed in the body frame." The least-squares solution then becomes

$${}_b\int p \, d\tau = \left({}_b\hat{U}\,{}_b\hat{U}^T\right)^{-1} \hat{U} \begin{pmatrix} m_1 \\ m_2 \\ m_3 \\ m_4 \end{pmatrix} = {}_b\hat{T}^t \left({}_t\hat{U}\,{}_t\hat{U}^T\right)^{-1} {}_t\hat{U} \begin{pmatrix} m_1 \\ m_2 \\ m_3 \\ m_4 \end{pmatrix} \tag{8}$$

Equation (8) holds for a general tetrad geometry. In the special geometry of the ortho-skew configuration, the following simplification results.

$${}_b\int \hat{p} \, d\tau = \left[\left({}_b\hat{T}^t \; {}_b\hat{u}_4\right) \begin{pmatrix} {}_t\hat{T}^b \\ {}_b\hat{u}_4^T \end{pmatrix} \right]^{-1} \left({}_b\hat{T}^t \; {}_b\hat{u}_4\right) \begin{pmatrix} m_1 \\ m_2 \\ m_3 \\ m_4 \end{pmatrix}$$

$$= {}_b\hat{T}^t \begin{pmatrix} m_1 \\ m_2 \\ m_3 \end{pmatrix} + \frac{1}{2}\, {}_b u_4 \left[m_4 - \cos\eta(m_1 + m_2 + m_3) \right] \tag{9}$$

Combining

$$\epsilon_5 = m_4 - \cos\eta(m_1 + m_2 + m_3) \tag{10}$$

and

$${}_b\hat{u}_4 = {}_b\hat{T}^t \begin{pmatrix} \cos\eta \\ \cos\eta \\ \cos\eta \end{pmatrix} \tag{11}$$

into equation (9), the least-squares output vector may be written

$${}_b\int \hat{p}\, d\tau = {}_b\hat{T}^t \begin{pmatrix} m_1 + (\epsilon_5 \cos\eta)/2 \\ m_2 + (\epsilon_5 \cos\eta)/2 \\ m_3 + (\epsilon_5 \cos\eta)/2 \end{pmatrix} \tag{12}$$

When a sensor failure has been detected and isolated, the mapping excludes the failed sensor. Denoting the unfailed sensor axes by u_i, u_j, u_k and corresponding measurements by m_i, m_j, m_k, the general solution becomes

$${}_b\int \hat{p}\, d\tau = ({}_b\hat{u}_i\ {}_b\hat{u}_j\ {}_b\hat{u}_k) \begin{pmatrix} m_i \\ m_j \\ m_k \end{pmatrix}$$

$$= {}_b\hat{T}^t ({}_t\hat{u}_i\ {}_t\hat{u}_j\ {}_t\hat{u}_k) \begin{pmatrix} m_i \\ m_j \\ m_k \end{pmatrix}$$

$$= {}_b\hat{T}^t \left[{}_t(\hat{u}_j \times \hat{u}_k) m_i + {}_t(\hat{u}_k \times \hat{u}_i) m_j + {}_t(\hat{u}_i \times \hat{u}_j) m_k \right] / (\hat{u}_i \times \hat{u}_j \cdot \hat{u}_k) \tag{13}$$

When the sensor geometry is restricted to the ortho-skew configuration and the failed sensor is removed, then the following simplification of (13) results:

$${}_b\int \hat{p}\, d\tau = {}_b\hat{T}^t \begin{pmatrix} m_1 \\ m_2 \\ m_3 \end{pmatrix} \quad \begin{matrix} \text{(No. 4 failed)} \\ \text{(skewed sensor)} \end{matrix} \tag{14}$$

$$ {}_b\int \hat{p}\, d\tau = {}_b\hat{T}^t \begin{pmatrix} m_4/\cos\eta - m_2 - m_3 \\ m_2 \\ m_3 \end{pmatrix} \quad \text{(No. 1 failed)} \tag{15} $$

$$ {}_b\int \hat{p}\, d\tau = {}_b\hat{T}^t \begin{pmatrix} m_1 \\ m_4/\cos\eta - m_1 - m_3 \\ m_3 \end{pmatrix} \quad \text{(No. 2 failed)} \tag{16} $$

$$ {}_b\int \hat{p}\, d\tau = {}_b\hat{T}^t \begin{pmatrix} m_1 \\ m_2 \\ m_4/\cos\eta - m_1 - m_2 \end{pmatrix} \quad \text{(No. 3 failed)} \tag{17} $$

Failure Detection by Parity Residual Sum Divergence

A theoretical relationship exists for any tetrad configuration that relates the measurements from the four like sensors:

$$ m_4 = \alpha m_1 + \beta m_2 + \gamma m_3 \tag{18} $$

Equation (18), which follows from equations (3) and (6), states that the output of any sensor can be formulated as a linear combination of the outputs of the other three sensors. This relationship is called parity. The coefficients α, β, γ are called parity coefficients. They can be determined from the tetrad's geometrical configuration. For the ortho-skew configuration,

$$ \alpha = \beta = \gamma = \cos\eta = 1/\sqrt{3} \tag{19} $$

More generally,

$$ \begin{pmatrix} \alpha \\ \beta \\ \gamma \end{pmatrix} = (\hat{u}_1\ \hat{u}_2\ \hat{u}_3)^{-1}\ \hat{u}_4 \tag{20} $$

Equation (18) never strictly holds in practice, hence a tetrad parity residual, ϵ_5, is defined as follows:

$$ \epsilon_5 = m_4 - \alpha m_1 - \beta m_2 - \gamma m_3 \tag{21} $$

Thus, ϵ_5 is the difference between the observed m_4 and the m_4 computed in equation (18). For a perfect system, ϵ_5 would always be zero in the absence of failures. Normal instrument errors and output quantization cause the parity residual to take on a small range of values in normal operation. When a failure occurs, the parity residual exceeds its normal range. Thus,

one can detect failures by monitoring ϵ_5. In this study, the parity residual is summed over a specified number of sequential data frames in order to detect small but persistent failures. These sequential data frames are called "accumulation interval for detection" or "detection window" and denoted by τ_d. The detection threshold d is the tolerance on the parity sum. A failure is indicated when the magnitude of the parity sum exceeds the detection threshold.

$$\text{Failure condition:} \quad \left| \sum^{\tau_d} \epsilon_5 \right| > d \tag{22}$$

The detection threshold and the length of the detection window determine the level of step failure which can be detected.

Figure 2 illustrates the failure detection procedure. The parity residual is computed for each set of four sensor measurements and is summed over the appropriate number of frames (τ_d) for comparison with the detection threshold. Figure 2 shows a step change in the parity residual, such as might result from a sensor failure. The change in the parity residual is the product of the step-failure size and the parity coefficient corresponding to the failed sensor. The parity residual sum increases the magnitude as a result of the step change in the parity residual, then levels out because the parity residual is summed over only the most recent τ_d data frames. If the failure is severe enough to cause the parity residual sum to exceed the detection threshold, the detection logic indicates a failure to the system.

The measurements m_i used in the computation of the parity residual must be appropriately compensated for biases, scale factors, and other known effects, or else the parity residual sum will indicate false failures. The effect of misalignment errors on the parity residual is to cause the parity coefficients to be in error. The parity coefficients are computed from the best estimates of the orientations of the sensors, but the measurements will be made by the sensors in their actual orientations. The differences between the estimated and actual orientations are misalignment errors. The coefficients, computed as in equation (19), depend on the orientations of all four sensors even though the coefficients multiply only three measurements in the parity residual. A bias-compensation error affects the parity residual in proportion to the coefficient it multiplies. That is, a bias error in sensor No. 4 contributes to the parity residual directly, while a bias error, $\tilde{b}$, in sensor No. 3 contributes $-\gamma\tilde{b}$ to the parity residual. Thus for the orthoskew configuration, a bias error of one unit in sensor No. 4 is equivalent to a bias error of $\sqrt{3}$ units in any one of the other three sensors in its effect on the parity residual. Of course, if a bias error is too large relative to the detection threshold, it will cause a false failure indication. For example, if the estimated scale factor of sensor No. 2 is in error by $\tilde{s}$, the corresponding contribution to the parity residual will be $-\tilde{s}\beta m_2$. As with biases, scale factor compensation errors can cause false alarms. Random measurement errors which have small means and variances relative to the quantization level will not significantly affect the parity sum.

The detection of a failure in a tetrad inertial sensor unit is a simple operation of calculation of the parity sum from accumulation of the parity

residual. When the magnitude of the parity residual sum exceeds the preset detection threshold, a failure is indicated. The minimum level of step error that can be detected is determined by the number of points in the parity residual sum and the size of the detection threshold.

Failed-Sensor Identification Algorithms

A tetrad strap-down inertial system inherently possesses fail-safe capability by virtue of the failure-detection capability just discussed. Extension to fail-operational, fail-safe capability requires the following:

1. A reliable algorithm for determining which instrument has failed when the failure-detection scheme indicates a failure. (The failure can then be removed from usage in subsequent calculations.)

2. An algorithm for detection of a failure in the three remaining instruments.

3. A confidence algorithm to preclude the erroneous identification of a good sensor rather than the faulty sensor.

Two failed-sensor identification algorithms have been investigated, each using measurement prediction in their computations. These algorithms, called the pseudosensor (PS) algorithm and the constrained-fit (CF) algorithm, are applied jointly to determine which sensor has failed.

Pseudosensor algorithm — If a fifth sensor of each type were available (i.e., a pentad configuration) each of five parity residual equations could combine the measurements of four sensors and exclude one sensor. Thus, extra parity residual equations would be used to identify the faulty sensor. If ϵ_i is the parity residual excluding m_i, the parity residual equations would be of the form:

$$\begin{pmatrix} \epsilon_1 \\ \epsilon_2 \\ \epsilon_3 \\ \epsilon_4 \\ \epsilon_5 \end{pmatrix} = \begin{pmatrix} 0 & -a_{12} & -a_{13} & -a_{14} & 1 \\ -a_{21} & 0 & -a_{23} & -a_{24} & 1 \\ -a_{31} & -a_{32} & 0 & -a_{34} & 1 \\ -a_{41} & -a_{42} & -a_{43} & 0 & 1 \\ -a_{51} & -a_{52} & -a_{53} & 1 & 0 \end{pmatrix} \begin{pmatrix} m_1 \\ m_2 \\ m_3 \\ m_4 \\ m_5 \end{pmatrix} \tag{23}$$

The equation for ϵ_5 excludes m_5 and may be recognized as the tetrad parity residual defined earlier in equation (21). Pentad (five-sensor) failure identification utilizes the five parity residuals, ϵ_i. If sensor i fails, ϵ_i will be smaller than any of the other parity residuals because m_i, the measurement which is in error due to the failure, enters each of the pentad parity residual equations except the equation for ϵ_i. Sensor i is thus identified as the failed sensor.

In the pseudosensor algorithm a fifth sensor is assumed whose predicted output, $\hat{m}_5$, is used in the first four pentad parity residual equations to identify the failed sensor. Correct identification is limited by the ability to predict $\hat{m}_5$. The fifth parity residual is used only for detection because it is the only parity residual computed from independent sensor outputs.

In the absence of failures (i.e., prior to the detection of a failure in the tetrad configuration), the pseudosensor's output, m_5, may be computed from the measurements of the four real sensors:

$$m_5 = {}_b u_5 \cdot {}_b\int \hat{p}\, d\tau$$

$$= c_{51} m_1 + c_{52} m_2 + c_{53} m_3 + c_{54} m_4 \tag{24}$$

The coefficients in equation (24) are defined by the geometry of the sensing axes of the real sensors and the sensing axis (i.e., ${}_b u_5$) chosen for the pseudosensor.

$$\begin{pmatrix} c_{51} & c_{52} & c_{53} & c_{54} \end{pmatrix} = {}_b u_5 \left({}_b\hat{U}\ {}_b\hat{U}^T \right)^{-1} {}_b\hat{U} \tag{25}$$

When a failure is detected, stored past values of m_5 are used in a least-squares fit to obtain polynomial coefficients with which to predict $\hat{m}_5$.

$$\hat{m}_5(t) = b_{50} + b_{51}(t - t_0) + b_{52}(t - t_0)^2 + \ldots + b_{5p}(t - t_0)^p \tag{26}$$

The least-squares fit should be based on recent data, but should not include data taken after the failure occurred. The exact time of the failure is sometimes difficult or impossible to ascertain. The apparent time of failure can be inferred by summing the parity residual backwards from the time of failure detection until this sum exceeds a present tolerance level; the most recent parity residual is added to the next most recent, etc. This process requires either that the past individual parity residuals or past sensor readings be stored in the computer. The number of points required for the backward sum to exceed the preset threshold level indicates the apparent time of failure relative to the point of detection. The interval of time between the apparent time of failure and the time of detection is the isolation interval for identification, τ_i. The detection window τ_d is greater than or equal to the number of points in the backward sum; otherwise, the failure would not have been detected in τ_d. The length, τ_f, of the fit interval and the polynomial order of the fit were chosen experimentally for this paper to optimize failure isolation success.

Using data from the fit interval to predict the output of the pseudosensor in the isolation interval τ_i, the first four pentad parity residuals, equation (23), are evaluated. These residuals are summed across τ_i and the smallest sum in magnitude is identified as corresponding to the failed sensor. Figure 3 illustrates the pseudosensor algorithm.

The situation shown in figure 3 is for a failure of sensor No. 3. The failure is detected at time t_d. The apparent time of failure is shown as four frames earlier, or $t_d - 4\Delta$. Pseudosensor fit coefficients are computed in the fit interval τ_f which includes the fit reference time, t_0. The four pseudosensor parity residuals, ϵ_i, are summed across the isolation interval, τ_i. The failure causes three of these sums to diverge more dramatically from zero than does $\Sigma\epsilon_3$; $\Sigma\epsilon_3$ exhibits some divergence, primarily because of prediction error. The rate of divergence of each of the other parity residual sums is approximately proportional to the failure level times the parity coefficient (eq. (23)) which multiplies m_3. The prediction error enters each parity residual sum equally, but may tend to reduce certain sums more than others because of sign differences in failure-induced divergence.

In summary, the pseudosensor algorithm:

1. Sums the tetrad parity residual, ϵ_5, backward from the time of detection to determine the apparent point of failure and the length of the isolation interval for identification, τ_i

2. Uses stored m_5 data computed from equation (24) to calculate coefficients of a polynomial (26) for the estimated pseudosensor output for use in the isolation interval

3. Extrapolates the polynomial to obtain predicted values of $\hat{m}_5$ to be used in the pseudosensor parity residual sum equations (23) in the isolation interval

4. Evaluates and integrates the pseudosensor parity residual sums, $\Sigma\epsilon_i$, ($i = 1, 2, 3, 4$) over τ_i identifying the failed sensor as the one whose parity residual sum is smallest in absolute value

The ability of the pseudosensor algorithm to correctly identify the failed sensor is limited by the ability to predict the output of the pseudosensor across the isolation interval for identification, τ_{2i}. The tendency of prediction errors to grow restricts the length of τ_i. Prediction errors will cause the four pseudosensor parity sums, $\Sigma\epsilon_1$ through $\Sigma\epsilon_4$, to diverge from zero, even in the absence of failures, making faulted-sensor identification difficult. If the prediction errors are adequately minimized, then one of the parity residual sums ($\Sigma\epsilon_3$ in fig. 3) will not diverge as rapidly as the others, thus making failed-sensor identification possible. The pseudosensor parity coefficients, a_{ij} in equation (23), are geometry-dependent. They are derived similarly to the tetrad parity coefficients, equation (20), except that the pseudosensing axis, ${}_bu_5$, enters their definition while one of the actual tetrad axes is excluded. The pseudosensor's axis must not be parallel to any tetrad axis or in the plane of any two tetrad axes. For example, if the aircraft's yaw axis is chosen for the pseudosensor from consideration of smoothness and predictability, the ortho-skew tetrad frame must be rotated away from the body (i.e., aircraft) frame.

The numerical values of the pseudosensor parity coefficients depend on the tetrad configuration as well as the relative orientation of the pseudosensor. It is desirable that all the coefficients a_{ij} be approximately equal

in magnitude (for equitable identification because of the dependence of parity residual-sum divergence rate on these coefficients). An optimal orientation of the ortho-skew tetrad frame (i.e., optimal ${}_bT^t$) was derived for which the largest ratio of any two coefficients was about 3.3. The pseudosensor algorithm is therefore unavoidably biased toward selecting some sensors as failed over others because the parity residual-sum divergence rates differ for the same failure level.

Constrained-fit algorithm — The basic idea behind the constrained-fit algorithm is that the measurement residual (i.e., difference between a sensor's observed and predicted measurements in the isolation interval, τ_i, will be greater for the failed sensor than for any of the unfailed sensors. This strategy, therefore, also requires prediction of sensor output readings in the isolation interval. Data points in the fit interval τ_f are used in a constrained polynomial fit for each sensor. The constraint imposed on the polynomial fitting procedure is that the polynomials must obey the parity equation (18) at all times. The fit constraint helps to smooth out noise and quantization error in the individual sensor measurements which might corrupt an unconstrained fit to the measurements. The fit constraint also tends to outweigh the effects of failed data which may lie in the fit interval because three unfailed sensors "out-vote" the failed sensor through the constraint. The apparent point of failure and the isolation interval are determined by summing the parity residual backward from the point of detection as in the pseudosensor algorithm. The fit interval ends at the point before the isolation interval begins.

The predicted measurement of the ith sensor at time t is given by

$$\hat{m}_i(t) = b_{i0} + b_{i1}(t-t_0) + b_{i2}(t-t_0)^2 + \ldots + b_{ip}(t-t_0)^p \qquad (27)$$

where the coefficients b_{ij} are evaluated from measured sensor data in the fit interval. Equations for the b_{ij} will be presented later. Equation (27) is used to predict each sensor's output in the isolation interval. The residuals δ_i, which correspond to the difference between the actual sensor output in the isolation interval and that predicted by the polynomial coefficients

$$\delta_i = m_i(t) - \hat{m}_i(t) \qquad (28)$$

are summed across τ_i, leading to a largest (absolute) sum for one of the sensors. The largest residual sum identifies the failed sensor.

Figure 4 illustrates the constrained-fit algorithm. The measurement residual sums, $\Sigma\delta_i$, are shown as functions of time in the isolation interval, τ_i. Three of these sums wander away from zero as a result of prediction errors. The fourth, that of sensor No. 3, is shown to diverge more rapidly away from zero. As with the pseudosensor algorithm, prediction errors can mask the divergence of relatively small failures and cause mistakes in identification of the failed sensor.

The constrained fit is a least-squares polynomial fit for which the coefficients obey a linear constraint. The constrained polynomial obeys the condition

$$\hat{m}_4(t) = \alpha\hat{m}_1(t) + \beta\hat{m}_2(t) + \gamma\hat{m}_3(t) \tag{29}$$

for t in the fit interval and in the isolation interval. Equation (29) is the tetrad measurement parity equation. The factors α, β and γ are the tetrad parity coefficients. Equation (29) conditions the coefficients of each order as shown in equation (30).

$$b_{4j} = \alpha b_{1j} + \beta b_{2j} + \gamma b_{3j} \tag{30}$$

This condition reduces the problem to finding b_{ij} for $i=1,2,3$ rather than for $i=1,2,3,4$. Equation (27) may be written in matrix form as shown in equation (31),

$$\hat{m}(\tau) = H(\tau)B \tag{31}$$

where

$$\hat{m}(\tau) = \begin{pmatrix} m_1(\tau) \\ m_2(\tau) \\ m_3(\tau) \\ m_4(\tau) \end{pmatrix} \tag{32}$$

$$H(\tau) = \begin{pmatrix} 1 & 0 & 0 & \tau & 0 & 0 & \tau^2 & 0 & 0 & \cdots \\ 0 & 1 & 0 & 0 & \tau & 0 & 0 & \tau^2 & 0 & \cdots \\ 0 & 0 & 1 & 0 & 0 & \tau & 0 & 0 & \tau^2 & \cdots \\ \alpha & \beta & \gamma & \alpha\tau & \beta\tau & \gamma\tau & \alpha\tau^2 & \beta\tau^2 & \gamma\tau^2 & \cdots \end{pmatrix} \tag{33}$$

$$B = \begin{pmatrix} b_{10} \\ b_{20} \\ b_{30} \\ b_{11} \\ b_{21} \\ b_{31} \\ b_{12} \\ b_{22} \\ b_{32} \\ \vdots \end{pmatrix} \tag{34}$$

and where $\tau = t - t_0$.

The fit interval is divided into n equal-length segments, each of length Δ, ($n\Delta = \tau_f$). Recent measurements from the four sensors, having been stored previously, are available for use in the fit. A four-vector, $m(\tau)$, whose elements are the four real measurements at τ, is defined analogously to equation (32). A measurement residual vector, Y, is defined by equation (35).

$$Y = \begin{pmatrix} m(\Delta) - \hat{m}(\Delta) \\ m(2\Delta) - \hat{m}(2\Delta) \\ \vdots \\ m(n\Delta) - \hat{m}(n\Delta) \end{pmatrix} = \begin{pmatrix} m(\Delta) \\ m(2\Delta) \\ \vdots \\ m(n\Delta) \end{pmatrix} - \begin{pmatrix} H(\Delta) \\ H(2\Delta) \\ \vdots \\ H(n\Delta) \end{pmatrix} B \tag{35}$$

where $m(\tau)$ is the actual sensor output and $\hat{m}(\tau)$ is the estimated output computed in the fit interval, τ_f. A least-squares fit minimizes Y^TY by optimizing in the fit interval, which is the objective of the constrained-fit strategy. The matrix solution for B is

$$B = (G^TG)^{-1}G^T \begin{pmatrix} m(\Delta) \\ m(2\Delta) \\ \vdots \\ m(n\Delta) \end{pmatrix} \tag{36}$$

where

$$G = \begin{pmatrix} H(\Delta) \\ H(2\Delta) \\ \vdots \\ H(n\Delta) \end{pmatrix} \tag{37}$$

and $H(\tau)$ was defined in equation (33).

The polynomial coefficients, B, computed by equation (36), are used in equation (27) to predict the estimated sensor output, $\hat{m}_i$, in the isolation interval, τ_i. The residual between the actual sensor output and the estimated sensor output is computed as in equation (28), then summed across τ_i.

The matrix, G, defined by equation (37), is a ($4n$ x $3p$) matrix, where p is the order of the polynomial and n is the number of points in the fit interval; G^TG is a ($3p$ x $3p$) matrix which must be inverted to compute B. It can be shown that the more convenient computational solution,

$$B = P^{-1}C \tag{38}$$

holds, where P^{-1} is the inverse of the symmetric ($p+1$) x ($p+1$) matrix,

$$P = \begin{pmatrix} n & \Delta\Sigma i & \Delta^2\Sigma i^2 & \cdots \\ \Delta\Sigma i & \Delta^2\Sigma i^2 & \Delta^3\Sigma i^3 & \cdots \\ \Delta^2\Sigma i^2 & \Delta^3\Sigma i^3 & \Delta^4\Sigma i^4 & \cdots \\ \cdots & \cdots & \cdots & \cdots \end{pmatrix} \tag{39}$$

in which the indicated summations are for $i = 1,2,\ldots,n$. The vector, C, in equation (38) is $3(p+1)$ - dimensional. Its elements, c^j, are 3-dimensional vectors defined by

$$c^j = \begin{pmatrix} \Sigma(i\Delta)^j m_1(i\Delta) \\ \Sigma(i\Delta)^j m_2(i\Delta) \\ \Sigma(i\Delta)^j m_3(i\Delta) \end{pmatrix} + \frac{1}{2}\,\Sigma(i\Delta)^j \epsilon_5(i\Delta) \begin{pmatrix} \alpha \\ \beta \\ \gamma \end{pmatrix} \tag{40}$$

where $\epsilon_5(i\Delta)$ is the tetrad parity residual at time $i\Delta$ relative to the fit reference.

Detection of Second Failures

Once a failure has been detected and the failed sensor identified, there are only three operational sensors remaining. Some mechanization is required for detecting a failure in one of the remaining sensors if the once-failed system is to be fail-safe. An adaptation of the pseudosensor algorithm scheme can be used to fill this need. A pseudosensor measurement is generated from the measurements of the three unfailed sensors at each time-point following detection and isolation of the first failure.

$$m_5 = c'_{5i} m_i + c'_{5j} m_j + c'_{5k} m_k \tag{41}$$

A recursive least-squares fit can be implemented to predict $\hat{m}_5$, using recent-past data over a specified interval which does not include the current point, in a manner similar to the generation of $\hat{m}_5$ with four good sensors.

$$m_5(\tau) = b'_{50} + b'_{51}\tau + b'_{52}\tau^2 + \ldots + b'_{5p}\tau^p \tag{42}$$

The b'_{5j} are computed by a least-squares fit to recent-past values of m_5. A failure is indicated when the magnitude of the pseudoresidual, δ_5, defined by

$$\delta_5 = m_5 - \hat{m}_5 \tag{43}$$

exceeds a preset tolerance. If a second failure is not indicated, the current measurements are used to update the polynomial coefficients b'_{5j} for the next time frame. This algorithm can only be valid when the aircraft's motion is smooth enough to be predictable in the near term.

Confidence Algorithm

The operation of the pseudosensor and the constrained-fit identification algorithms is subject to incorrect solution for small failures and for large failures in conjunction with large amplitude high-frequency angular motion, such as may occur in abrupt turns or in severe turbulence. For this reason, a confidence algorithm was developed to test and reject these incorrect solutions. It is better to only indicate the presence of a failure than to identify a good sensor as a bad one and leave faulty data in the computational process. That is, the effects of small failures in one sensor of a tetrad inertial sensing unit are reduced (see eqs. (8) and (12)) in their influence on the triad output by the three good sensors, but if good data are removed by mistake, the faulty data have increased influence (see eqs. (13) through (17)) on the output. The indication of an unidentified failed sensor can show that the system's performance will be degraded. (The tetrad for these small failures has only an FS capability.)

A confidence algorithm with 12 confidence measures was developed to judge the validity of the faulty sensor identification solution. These measures evaluate such questions as "How decisive is the solution, as judged by the pseudosensor parity residual sums?", "How good is the fit as judged by the fit residuals?" or "Do the pseudosensor and constrained-fit algorithm outputs agree?". These confidence measures, which are somewhat empirical in origin and derivation, often overlap each other in the nature of their tests. The 12 measures will be described, together with a mathematical statement of each test. Definitions of variables used in the tests will be found in the notation section.

Confidence measure No. 1 — The isolation interval must be short. In other words, detection must be immediate. Not only are sharp failures more likely to be correctly identified because of the implied failure size, but short prediction intervals aid in successful identification as well.

$$N < \lambda_1 \tag{44}$$

Confidence measure No. 2 — The apparent failure level must be large. Failure identification success improves when the failure is a high multiple of the failure-free parity residual noise level.

$$\bar{\epsilon}_5/\sigma_p > \lambda_2 \tag{45}$$

Confidence measure No. 3 — The apparent failure level must be large in comparison with the pseudosensor fit residual. Fit errors usually lead to prediction errors, but are not critical to the solution if the failure is sharp enough.

$$\left|\bar{\epsilon}_5/\alpha_{k_p}\right|/r_5 > \lambda_3 \tag{46}$$

Confidence measure No. 4 — The pseudosensor algorithm's outcome must be decisive. The pseudosensor algorithm determination of failure is based on

comparison among four parity residual sums. The smallest sum identifies the faulty sensor, but in marginal cases, the smallest sum may not differ very much from the next smallest sum. If the prediction error is small and the failure level is large, however, the smallest pseudosensor parity residual sum will be decisively smaller than the next smallest.

$$\left|\Sigma\epsilon_{ns}/\Sigma\epsilon_{min}\right| > \lambda_4 \tag{47}$$

Confidence measure No. 5 — The apparent failure level must be much larger than the apparent pseudosensor prediction error. The apparent prediction error is the value of the smallest parity residual in the isolation interval.

$$\left|\bar{\epsilon}_5/\alpha_{k_p}\right| \Big/ \left|\Sigma\epsilon_{min}/N\right| > \lambda_5 \tag{48}$$

Confidence measure No. 6 — The rms pseudosensor fit residual must be small. This measure is an absolute test of goodness-of-fit, normalized by the rms parity residual but not compared against apparent failure size.

$$r_5/\sigma_p < \lambda_6 \tag{49}$$

Confidence measure No. 7 — The apparent failure must be large in comparison to the largest constrained-fit rms fit residual. This measure is analogous to confidence measure No. 3, but for the constrained-fit strategy rather than for the pseudosensor strategy.

$$\left|\bar{\epsilon}_5/\alpha_{k_c}\right| \Big/ \max(\sigma_f) > \lambda_7 \tag{50}$$

Confidence measure No. 8 — The constrained-fit outcome must be decisive. This measure is analogous to measure No. 4.

$$\left|\Sigma\delta_{max}/\Sigma\delta_{n1}\right| > \lambda_8 \tag{51}$$

Confidence measure No. 9 — The maximum apparent constrained-fit prediction error must be small compared to the apparent failure level. This measure is analogous to measure No. 5.

$$\left|\bar{\epsilon}_5/\alpha_{k_c}\right| \Big/ \max(\sigma_i) > \lambda_9 \tag{52}$$

Confidence measure No. 10 — The apparently failed sensor's measurement residual in the isolation interval must be large. This measure overlaps measure No. 2 somewhat.

$$\sqrt{(\Sigma\delta_{max}/N)^2 - \left[\max(\sigma_i)\right]^2} \Big/ \sigma_p > \lambda_{10} \tag{53}$$

Confidence measure No. 11 — The rms constrained-fit residuals in the fit interval must be small. This measure, like measure No. 6, is an absolute test of goodness-of-fit, normalized but not compared with apparent failure size.

$$\max(\sigma_F)/\sigma_p < \lambda_{11} \tag{54}$$

Confidence measure No. 12 — The answers obtained by the two identification algorithms must agree.

$$k_c = k_p \tag{55}$$

Confidence measures No. 1 and No. 2 are independent of the identification algorithms. These measures assess the size of the failure and the rapidity by which it was apparently detected. (A ramp-type failure is more difficult to isolate.) Confidence measures Nos. 3 through 6 evaluate how believable the pseudosensor solution is. Confidence measures Nos. 7 through 11 evaluate the reliability of the solution for the constrained-fit algorithm. Confidence measure No. 12 compares the results of the two algorithms.

If any of the confidence measures are not satisfied by the computational tests, the identification solution is rejected and the system reverts to a fail-safe-only classification. The λ_i must be determined for the particular tetrad system under consideration, and determined such that no incorrect solutions will be accepted while very few correct solutions are rejected.

ASSESSMENT OF TETRAD FAILURE DETECTION, IDENTIFICATION, AND CONFIDENCE ALGORITHMS

Sensor Failures

The failure detection, identification, and confidence algorithms were tested using prerecorded experimental data (appendix) consisting of step failures introduced in the sensor outputs. As stated in the introduction, the ability of the identification algorithms to identify step failures is a necessary, but not sufficient condition, for flight control application. The failure step size was varied between 367°/hr and 4900°/hr. These step failures were inserted in four different test data regions which included simultaneous ramp and sinusoidal motion on different orthogonal axes. These experimental data are described in the appendix.

Sensor Response Prediction

The success of a possible tetrad FO-FS strategy depends on accurate prediction of the outputs of the individual sensors (constrained fit) and of the fifth sensor (pseudosensor) in the isolation interval from sensor data collected in the fit interval. Because of unpredictable aircraft motions, the predictions always contain errors. These errors can lead to an erroneous faulted sensor identification. The prediction error generally increases with increasing lengths of isolation (prediction) interval.

This error function is illustrated in figure 5, which shows the rms prediction error of the fifth sensor (the pseudosensor) as a function of isolation interval (i.e., prediction length). The figure displays the rms value of 80 samples of $(m_5 - \hat{m}_5)$ predicted one frame, two frames, ..., ten frames. The 80 samples were obtained by fitting five points to a straight line, where the fit reference point, t_0, was taken at each of 80 sequential points.

Practical judgments were required in setting the polynomial fit order and length of the fit interval for this experimental evaluation. Thresholds for failure detection and confidence measures must also be selected while considering the nature of the sensor data. Selection of fit order and the number of fit points depends on the frequency of the motion and the measurement sampling frequency as well as on the sensor quantization and noise levels. The experimental data were sampled every 0.128 sec (about 8 Hz). Gyro quantization was 24.5°/hr per count (bit) per data frame. The rms parity residual noise in the four regions varied from 1.5 to 2.0 counts per data frame. Ranges of fit order and fit interval length were tested to determine optimum values for this experimental evaluation. Fit orders 0, 1, and 2 were tried, along with 3, 5, and 7 points in the fit interval.

Table 1 presents the number of successful faulted-sensor identifications obtained from 2560 cases. The 2560 cases were made up of 80 time points, 8-step failures at each time point and for four different sensors. The 8-step failures ranged from 40 counts per data frame (980°/hr) to 180 counts per data frame (4410°/hr). Table 1 indicates that fits of order 1 (i.e., straight line) to three data points in the fit interval gave the best faulted-sensor isolation success for the cases tested. Table 2 presents the information of table 1 in percentages. Relative success of the straight-line fits to three or five data points is explained by the vehicle motion in the evaluation. Its frequency was higher than the measurement sampling frequency (8 samples/second) so that only a few data frames (e.g., 3 or 5) could be used in the fit interval. The motion was sufficiently time-variant that a zero-order fit was inadequate. Quantization of the sensor output and sensor measurement noise cause fitting mistakes for second-order and higher-order fits.

TABLE 1. — NUMBER OF SUCCESSFUL FAULTED-SENSOR IDENTIFICATIONS vs FIT ORDER AND FIT INTERVAL

Data frames in fit interval	Fit order		
	0	1	2
3	1728	2220	1792
5	1553	2130	2032
7	1783	2053	2016

TABLE 2. — PERCENT SUCCESSFUL FAULTED SENSOR IDENTIFICATIONS vs FIT ORDER AND FIT INTERVAL

Data frames in fit interval	Fit order		
	0	1	2
3	67.5%	86.7%	70.0%
5	60.7%	83.2%	79.4%
7	54.0%	80.2%	78.8%

The necessity for a good fit decreases as the failure level increases because the effect of fitting and prediction errors becomes relatively less influential on the outcome of the isolation strategies. Results in tables 1 and 2 indicate trends. These trends were used to select the polynomial fit order and the length of the fit interval for the detailed evaluation of the strategies. The three-point fit interval and first-order fit were shown to be the best fit (86.7% successful) for this case, but a five-point, first-order fit (83.2% successful) was chosen for later studies because the confidence measures for the five-point fit were slightly superior to those for the three-point fit.

A failure is indicated when the moving-window sum of the parity residuals equals or exceeds the threshold. For example, if the detection threshold was set at 980°/hr, then a step failure of 245°/hr in sensor No. 4 would cause a failure indication in four data frames (i.e., (4)(245°/hr) = 980°/hr). This detection threshold must be high enough to exclude "false alarms" yet low enough to trigger on minimum failures. Much smaller failures can be detected than one could expect to correctly isolate (i.e., identify) in a tetrad instrument package. Figure 6 indicates the number of frames required to exceed a preset detection threshold of 980°/hr for various step-failure levels. The data are presented for detection intervals from 1 to 10 data frames. Eighty test cases were run for each step-failure level. For example (refer to fig. 6), 80 different 200°/hr step failures were imposed on gyro No. 1 and a detection of these simulated failures occurred 15 times in the seventh frame following failure, 51 times in the eighth frame and 14 times in the ninth frame (for a total of 80). Similar failures are detected more rapidly in gyro No. 4 under the same conditions because of its larger coefficient (weighting factor) in the parity residual.

Confidence Algorithms Constants

The identification confidence measures (CM) require numerical constants in order to execute the algorithm for accepting or rejecting the decisions made by the pseudosensor and constrained-fit algorithms. The numerical constants are strongly related to the character of the experimental data.

Considerable computer processing of different values for the numerical constants (using the same experimental sensor data) was done to select the best values to be used in this study. The primary constraint used in selecting the numerical constants was that no false identifications be accepted by the confidence algorithm. Practical considerations led to the numerical values (thresholds) used in the confidence measures and shown in table 3. These values are not optimized, but represent the best performance that could be obtained during the study.

TABLE 3. -- CONFIDENCE THRESHOLDS, λ_i

i	λ_i	i	λ_i
1	4	7	4
2	20	8	2
3	6	9	3
4	2	10	30
5	4	11	3
6	3		

Performance Summary

There are four possible outcomes of the two faulted-sensor identification algorithms in connection with simulated failures. These four outcomes are:

(Y) Successful identification of the faulted sensor and acceptance of the solution

(N) Unsuccessful identification of the faulted sensor and rejection of the solution

(R) Successful identification of the faulted sensor and rejection of the solution

(U) Unsuccessful identification of the faulted sensor and acceptance of the solution.

The objectives of the tetrad strategy are to maximize the number of successful, accepted (Y) cases, minimize the number of unsuccessful (N) or rejected (R) cases, and have no unsuccessful-but-accepted (U) cases. The experimental results summarizing the performance are shown in table 4. These results illustrate the experimental performance of the tetrad strategy for simulated step failures. For step errors of 2940°/hr or greater, the isolation interval is one and the (Y) percentage of total cases is greater than 80%. For step errors smaller than 2940°/hr the isolation intervals are often greater than one data frame. The number of (N) and (R) cases also increases

TABLE 4. – PERFORMANCE SUMMARY OF TETRAD FO-FS REDUNDANCY MANAGEMENT STRATEGY

Gyro error, deg/hr	FDI[a]				FD2				FD3				FD4			
	Y[b]	N[c]	R[d]	U[e]	Y	N	R	U	Y	N	R	U	Y	N	R	U
367					0.0	1.9	0.6	0.0	0.0	18.4	4.7	0.0	0.0	55.6	18.7	0.0
490					.0	5.9	2.2			37.8	10.0			30.9	13.1	
612	0.0	0.0	0.3	0.0	.0	18.1	8.4			39.7	20.9			6.6	5.9	
735	.0	.0	1.6		.0	31.6	24.4			25.6	15.6			.9	.3	
980	3.1	5.6	11.6		.9	30.3	40.3			4.7	3.4					
1225	5.3	6.9	16.2		.0	11.2	51.6			2.5	.6					
1470	13.1	9.7	25.6		7.5	11.6	31.9			.6	.6					
1715	21.9	8.7	60.6		.3	2.2	6.2									
1960	35.9	11.6	49.4		1.2	.3	1.6									
2450	60.3	3.7	35.6		.0	.0	.3									
2940	83.4	.6	15.9													
3430	90.9	.6	8.4													
3920	95.6		4.4													
4410	99.1		.9													
4900	100.0		.0													

[a]FDI = ith data frame in isolation interval

[b]Y = successful and confidence measures accept decision (% of 320 samples)

[c]N = unsuccessful and confidence measures reject decision (% of 320 samples)

[d]R = successful but confidence measures reject decision (% of 320 samples)

[e]U = unsuccessful but confidence measures accept decision (% of 320 samples)

until, for failures smaller than 980°/hr, all cases are either (N) or (R). The results from table 4 are presented graphically in figures 7 and 8. Figure 7 shows the percentage of successful isolations (Y+R outcomes) and the percentage of successful-and-accepted isolations (Y outcomes only), versus failure level, without regard for the number of frames required to detect the failure. Figure 8 shows three histograms representing horizontal samples of the data from table 4. Each histogram pertains to a particular failure level (490°/hr, 980°/hr, and 1960°/hr are shown). A bar is shown for each frame. The total height of the bar at each frame is the percentage of cases detected in that frame. Each bar may contain "N", "R" and "Y" segments. In the histogram for 1960°/hr step failures, for example, nearly 97% of the failures were detected in one frame and about 85% of these were successfully isolated, although only about 36% were accepted. The other bars may be similarly interpreted. The tetrad strategy detected and accepted 100% of all step-failures larger than 4410°/hr and no unsuccessful solutions were accepted for the fit order and fit intervals chosen for this detailed study.

It is significant that no cases of type (U) occur, even for small failures. The confidence algorithm precludes an error in failed-sensor identification, but it also causes rejection of many successful isolations. These are shown in table 4 as (R)-type cases. The penalty for excluding all (U)-type cases is illustrated in figure 7, which shows the divergence between unqualified successful identifications and successful identifications accepted by the 12 confidence-measure algorithms. Relaxing the confidence-measure thresholds to accept more successful identifications will increase the likelihood of accepting wrong identifications unless the confidence algorithms are improved.

The percentage of (Y) cases can be increased by decreasing the quantization level, while increasing the quantization level degrades the isolation performance. This is shown in figure 9, the input data for which was simulated and noise-free. The practical value of the quantization level, q, is approximately 1.6 arcsec/count — a level currently available in laser gyros. The 99% confidently identifiable step-type failure at a 1.6 arcsec/count quantization level is about 500°/hr.

CONCLUDING REMARKS

It has been shown that for step failures of a given magnitude, the faulty sensor can be identified. For lower magnitude step failures the tetrad strategy does not identify the faulted sensor properly; however, the confidence algorithm indicates when the solution is suspect.

As has been shown in the development, four sensors are necessary for detecting (by parity) a failure. Additional information is needed in order to isolate which one of the four has failed. This study investigated the feasibility of using prediction techniques for gaining the required information for identifying sensor failures in the tetrad configuration.

An interesting by-product of this study was the problem of generating clean parity signals for the detection algorithm from experimental data.

Although the integrating rate gyro sensors were supposedly of inertial-grade quality, considerable computational effort was required to obtain clean enough signals for this study.

These problems suggest that using parity residuals for detection and isolation in pentad and hexad inertial reference systems requires considerable care in the calibration of the units. The instrument's output also has to be relatively free of noise with low quantization levels if parity residuals are to be useful in detecting small bias-offset-type failures with very small probability of false alarms.

APPENDIX

EXPERIMENTAL FACILITY AND DATA USED IN STUDY

The tetrad FO-FS strategy was tested with real sensor data generated on the facility shown in figure 10.

Facility Description

This facility was developed at Ames Research Center for testing redundancy management concepts applicable to strap-down inertial sensor systems. The facility includes a three-axis gimbaled table; a laboratory strap-down, variable angle, hexad inertial sensor assembly; a minicomputer; a digital magnetic tape recorder; and a line printer and other peripherals required for conveniently testing redundancy management concepts and strategies. The minicomputer is used for time-division multiplexed data acquisition and for driving the table.

The attitude table is an orthogonal three-axis, gimballed system controlled by an electro-hydraulic servo whose attitude inputs can be derived from typical V/STOL flight profiles prerecorded on magnetic tape, or by a function generator with sine wave, triangular wave, or ramp outputs at selected frequencies. Monitoring of gimbal angles is accomplished with high resolution linear Inductosyn digital shaft encoders whose angular resolution is 2.5 arcsec. The table is mounted on a concrete base 1.5 m (5 ft) in depth, which is in turn supported by 30.5 m (100 ft) pilings.

The variable angle hexad strap-down inertial sensor assembly shown in figure 11 is mounted on the attitude table in an ortho-skew tetrad configuration, with three sensor (gyro and accelerometer) pairs orthogonal to each other, and a fourth sensor pair skewed to a position which has equal angles to the three orthogonal axes. The gyros are Hamilton Standard Model RI1139 single-degree-of-freedom, pulse-rebalanced, rate-integrating wheel type, and the Singer-General Precision Model 2401 accelerometers are pulse-rebalanced, single-axis, pendulous devices. All the sensors were surplused from the Lunar Module Abort Guidance System of the NASA Apollo program.

The data acquisition system, schematically shown in figure 12, consists of 14 time-division multiplexed channels which are used to transmit both inertial sensor data and gimbal axis angular-position information from digital shaft encoders to the minicomputer for reprocessing. The formatted data are then transmitted to a digital magnetic-tape recorder and also to a line printer. The data acquisition system includes both A-D converter and D-A converter units for outputing to analog recorders or inputting from function generators or conventional tape.

Sensor data and digital shaft encoder data are transmitted to the computer via the multiplexer every 128 msec. The computer transmits these raw data to the digital magnetic-tape transport unit for use with off-line

redundancy management experiments, and also unpacks and scales the data for use with four different analysis programs. The data analysis programs in the minicomputer perform the following functions: parity-error computation, sensor cumulative count average, gyro error detection and a comparison of sensor and shaft encoder angular position information. The output of each program can be displayed on a line printer for quick-look analysis.

Inertial Sensor Calibration

Output signals of gyros and accelerometers must be compensated for non-zero biases, non-unit scale factors, axis misalignments and other effects in order to be made useful in either a flight control or navigation system. Calibration was accomplished using static and dynamic methods. In a stationary condition, gyros measure Earth's rotation rate and accelerometers measure gravitational reaction. Wheel gyro output is affected by gravity because of wheel mass unbalance. The calibration procedure was formulated by a measurement model which related the estimated input and measured sensor output through the compensation parameters. Equations (A1) and (A2), which are the same as equations (4) and (5) but repeated here for the reader's convenience, illustrate the measurement models:

Attitude gyro measurement model:

$$\Delta\theta_i(t) = \left\{ \int_{t-\Delta}^{t} (b_i + S_i \cdot \Omega + M_i \cdot F)d\tau + \tilde{q}_i + \tilde{r}_i \right\} \tag{A1}$$

Accelerometer measurement model:

$$\Delta v_i(t) = \left\{ \int_{t-\Delta}^{t} (b_i + S_i \cdot F)d\tau + \tilde{q}_i + \tilde{r}_i \right\} \tag{A2}$$

Compensation parameters are: biases (b_i), scale factor and alignment vectors (S_i) and, for the gyros, mass unbalance vectors (M_i). Inertial sensor outputs and three-axis table attitude angles are recorded for a number of prescribed static orientations. A standard least-squares procedure is used to determine those compensation parameter values which minimize the sum-squared difference between estimated and observed sensor outputs. Measurement noise and quantization effects are accommodated by averaging the sensor outputs over a 20-min interval at each static orientation.

The scale factor and alignment vectors, S_i, for the gyros are determined by a dynamic calibration procedure in which the attitude table is rotated through a given angle about each gimbal axis in sequence. Gyro outputs are approximately proportional to the component of rotation along the gyro's input axis. This relationship permits calibration of S_i using a finite rotation sequence. The two methods are shown schematically in figure 13 and the resultant calibrated compensation parameters are shown in table 5.

TABLE 5.- SENSOR COMPENSATION PARAMETERS

	Bias, b_i (counts)	Scale factor-alignment vector, S_i (counts/deg or counts/g)		Parity coefficients
Gyro No. 1 (α)	-0.36435	10.30	-0.61	-1117.97 - 0.66035
Gyro No. 2 (β)	-.15447	40.40	1123.62	-1.02 - .63636
Gyro No. 3 (γ)	.01053	-1090.40	35.06	-92.47 + .6601
Gyro No. 4 (1)	.13842	752.35	691.46	-667.86 1.0000
Accel No. 1 (α)	1.24	-5.40	2.02	-1290.55 - .57213
Accel No. 2 (β)	-18.09	39.94	1311.82	-27.87 - .55180
Accel No. 3 (γ)	.54	1258.06	-33.17	-133.36 - .58508
Accel No. 4 (1)	-7.96	755.01	705.61	-831.77 1.0000

Note: The gyro mass unbalance compensation parameters used in this paper were zero.

The tetrad parity residual, ε_5, of equation (A3) is a direct measure of the "goodness" of the calibration.

$$\varepsilon_5 = m_4 - \alpha m_1 - \beta m_2 - \gamma m_3 \qquad \text{(A3)}$$

If the estimated bias of any one sensor is in error, the average parity residual will be proportionately offset from zero. The parity coefficients α, β, and γ, which are computed from the estimated scale factor and alignment vectors S_i, must be very accurate or the gyro parity residual will fluctuate wildly in the presence of large angular rates. The parity residual bias error determines the failure-detection sensitivity and the minimum isolatable failure level. These derived parity coefficients are shown in table 5.

Tetrad Experimental Data

Figures 14-16 show the actual gyro data used to evaluate the tetrad FO-FS algorithms. The gyros were mounted on the motion table which was commanded to undergo oscillatory angular motion about two axes-roll and pitch. The gyro output shown in the figures represents digitized integrated angular rate sensed as a result of this motion.

The apparently continuous curves shown in the figures are really discrete points connected artificially by the plotting routine. The discrete points are sensed angular rate integrated over one data frame (0.128 sec) by each gyro. Oscillatory angular motion was selected as a convenient way to introduce variable, flight-similar angular rates to be measured by the gyros. The period of the commanded oscillatory motion was chosen as 5-10 sec for roll and 100 sec for pitch. Amplitudes of the motion were chosen as 4° in roll and 20° in pitch. This motion was well within the capabilities of the table and, though not a perfect simulation of aircraft motion, developed rates and rate variations which might be encountered in aircraft flight. Irregularities in the table drive system produced irregular rate variations, especially noticeable in the pitch (outer gimbal) axis, which degraded performance of the failure isolation algorithms. These irregular rate variations are believed to pose a more severe test of the failure isolation algorithms than real aircraft motion would pose.

Gyro data from four different regions (I, II, III, and IV) of the data displayed in figures 14-16 were used to test the algorithms. Shown on each figure is the parity residual computed from the raw sensor data and the sensor compensation parameters from calibration. The parity residuals showed no observable bias, a noise level of between 24.5°/hr and 49°/hr and a motion dependency (e.g., scale factor misalignment or mass unbalance error) of about 1%.

Region I, shown in figure 14, represents a roll oscillation of 0.1 Hz and no pitch or yaw motion. The pitch gyro, whose axis was not perfectly orthogonal to the roll axis, exhibits a small component of roll rate while the skewed gyro exhibits a sizable component of roll rate. The rolling motion includes both (commanded) and high (resultant) frequency components. The peak roll was approximately 4000°/hr.

Region II, shown in figure 15, includes a rolling oscillation similar to that of Region I, a pitch rate with high frequency jitter, and no yaw motion. Region III, also shown in figure 15, includes low- and high-frequency variation in pitch and roll and no yaw motion. The maximum pitch rate was about 6400°/hr. Region IV, shown in figure 16, includes a linearly changing roll rate from about +7800°/hr to -8300°/hr, a relatively constant pitch rate of 1900°/hr, and no yaw motion. Each region was about 3-sec long and provided 20 separate data frames.

REFERENCES

1. Eberlein, A. J.; and Savage, P. G.: Strapdown Cost Trend Study and Forecast. NASA CR-137585, Oct. 1975.

2. Gilmore, J. P.: A Non-Orthogonal Gyro Configuration. MIT MS Thesis, Jan. 1967.

3. Musoff, Howard: SIRU Utilization, Volume I, Theory, Development and Test Evaluation. R-747, The Charles Stark Draper Laboratory, Mar. 1974.

4. Gilmore, J. P.; and Cooper, R. J.: SIRU Development-Final Report. R-746, The Charles Stark Draper Laboratory, July 1973.

5. Wilcox, J. C.: Competitive Evaluation of Failure Detection Algorithms for Strapdown Redundant Inertial Instruments. TRW Report No. 18313-6004-RU-00, April 1973 (NAS8-27335).

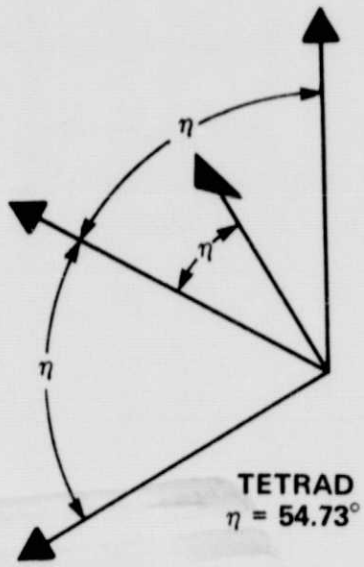

Figure 1.- Ortho-skew tetrad sensor configuration.

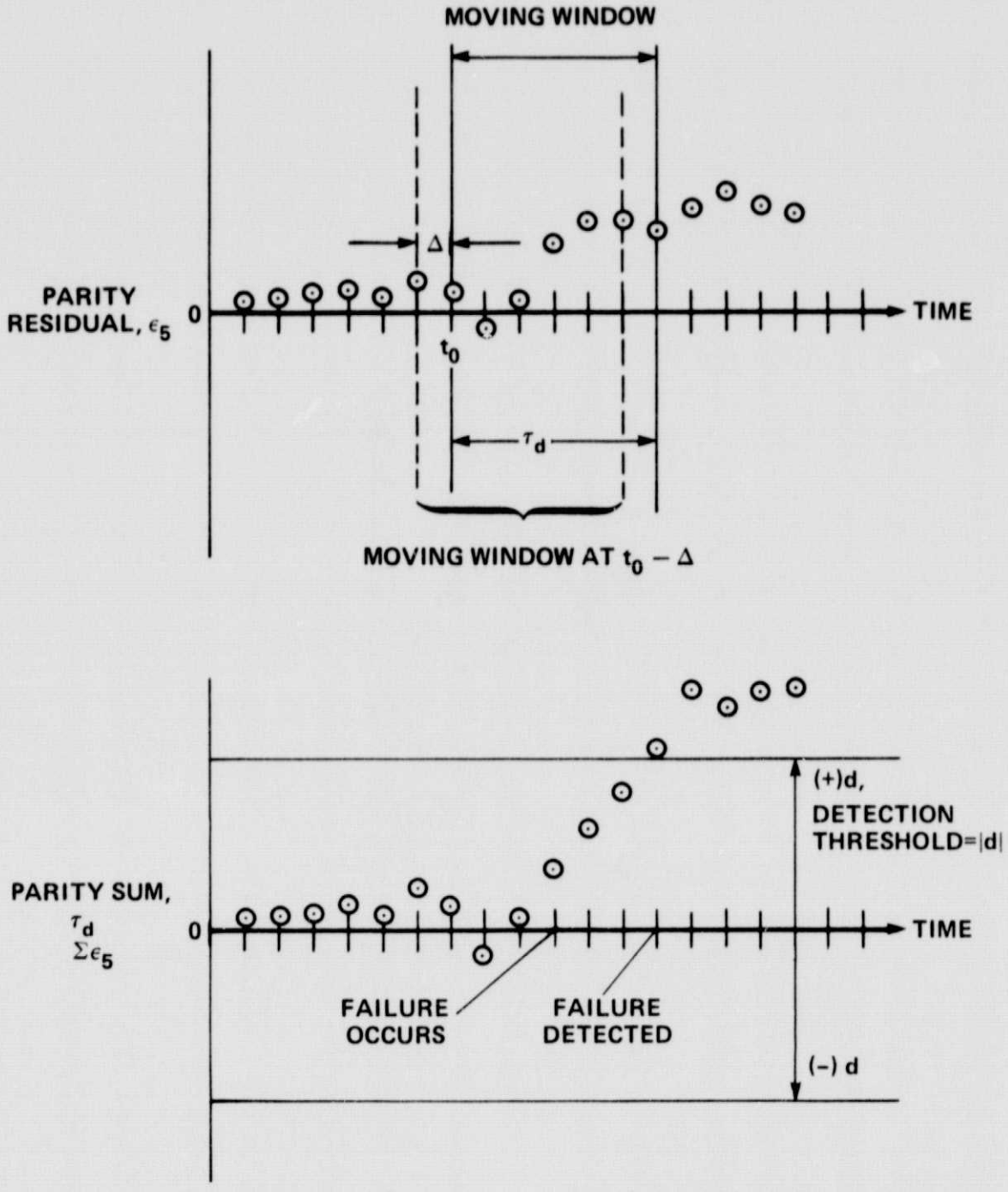

Figure 2.- Tetrad failure detection procedure.

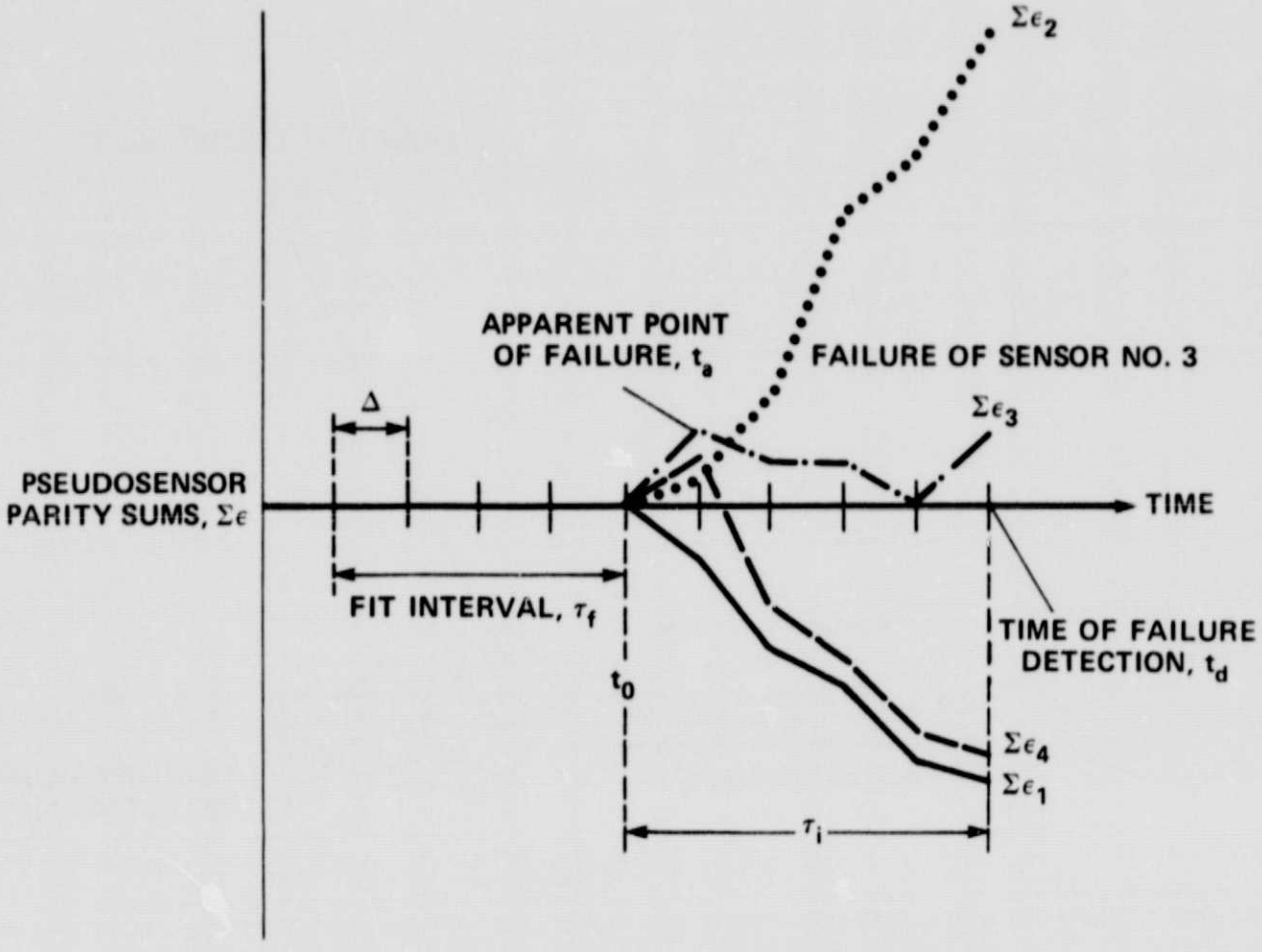

Figure 3.- Pseudosensor strategy.

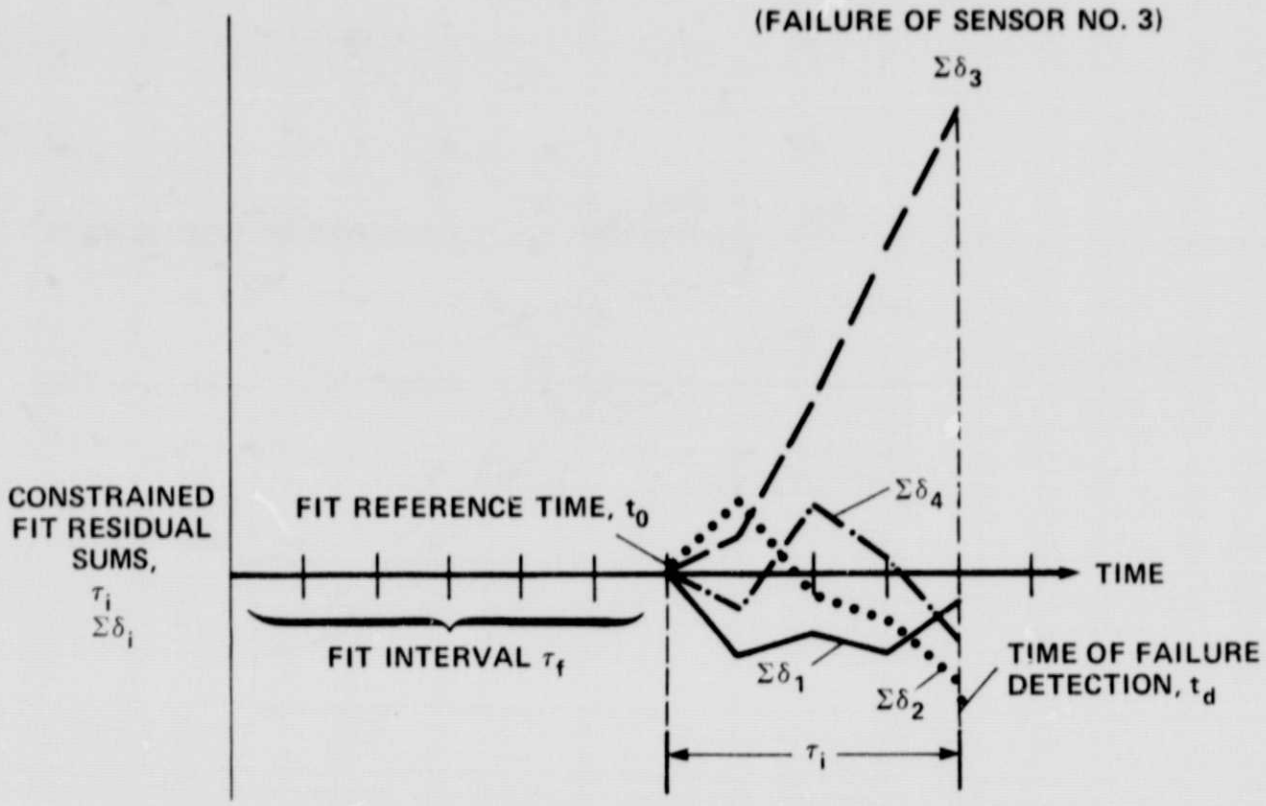

Figure 4.- Constrained-fit strategy.

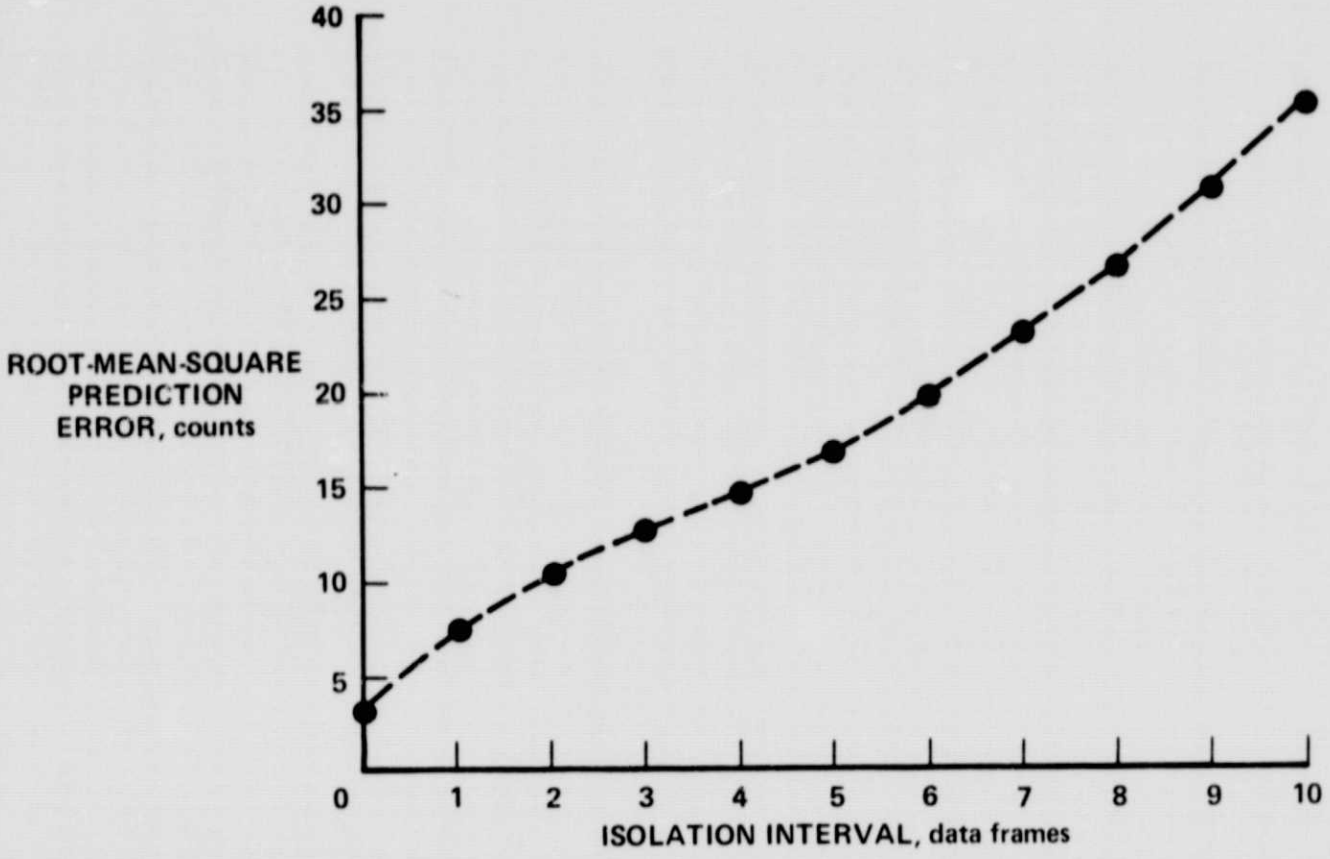

Figure 5.- Root-mean-square error in prediction of the pseudosensor's output vs number of data frames in the isolation interval (5-point, first-order fit in region I).

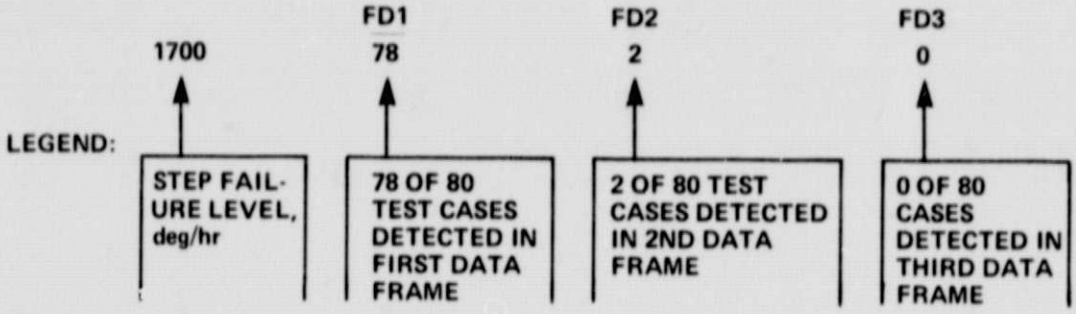

Step failure level	Gyro 1										Gyro 2										Gyro 3										Gyro 4									
deg/hr	1	2	3	4	5	6	7	8	9	10+	1	2	3	4	5	6	7	8	9	10+	1	2	3	4	5	6	7	8	9	10+	1	2	3	4	5	6	7	8	9	10+
50.	0	0	0	0	0	0	0	0	0	80	0	0	0	0	0	0	0	0	0	80	0	0	0	0	0	0	0	0	0	80	0	0	0	0	0	0	0	0	0	80
100.	0	0	0	0	0	0	0	0	0	80	0	0	0	0	0	0	0	0	0	80	0	0	0	0	0	0	0	0	0	80	0	0	0	0	0	0	0	0	14	66
150.	0	0	0	0	0	0	0	0	7	73	0	0	0	0	0	0	0	0	3	77	0	0	0	0	0	0	0	0	11	69	0	0	0	0	0	14	55	11	0	0
200.	0	0	0	0	0	0	15	51	14	0	0	0	0	0	0	0	6	48	26	0	0	0	0	0	0	0	20	48	12	0	0	0	0	0	48	32	0	0	0	0
250.	0	0	0	0	0	45	35	0	0	0	0	0	0	0	0	29	49	2	0	0	0	0	0	0	1	44	35	0	0	0	0	0	0	48	32	0	0	0	0	0
300.	0	0	0	0	45	35	0	0	0	0	0	0	0	0	30	50	0	0	0	0	0	0	0	0	45	35	0	0	0	0	0	0	14	66	0	0	0	0	0	0
350.	0	0	0	16	64	0	0	0	0	0	0	0	0	8	70	2	0	0	0	0	0	0	0	20	60	0	0	0	0	0	0	0	67	13	0	0	0	0	0	0
400.	0	0	0	66	14	0	0	0	0	0	0	0	0	54	26	0	0	0	0	0	0	0	0	68	12	0	0	0	0	0	0	0	80	0	0	0	0	0	0	0
450.	0	0	9	71	0	0	0	0	0	0	0	0	5	75	0	0	0	0	0	0	0	0	11	69	0	0	0	0	0	0	0	14	66	0	0	0	0	0	0	0
500.	0	0	45	35	0	0	0	0	0	0	0	0	30	50	0	0	0	0	0	0	0	0	45	35	0	0	0	0	0	0	0	49	31	0	0	0	0	0	0	0
550.	0	0	73	7	0	0	0	0	0	0	0	0	63	17	0	0	0	0	0	0	0	0	75	5	0	0	0	0	0	0	0	75	5	0	0	0	0	0	0	0
600.	0	0	80	0	0	0	0	0	0	0	0	0	80	0	0	0	0	0	0	0	0	0	80	0	0	0	0	0	0	0	0	80	0	0	0	0	0	0	0	0
650.	0	5	75	0	0	0	0	0	0	0	0	1	79	0	0	0	0	0	0	0	0	3	77	0	0	0	0	0	0	0	0	80	0	0	0	0	0	0	0	0
700.	0	16	64	0	0	0	0	0	0	0	0	8	72	0	0	0	0	0	0	0	0	20	60	0	0	0	0	0	0	0	0	80	0	0	0	0	0	0	0	0
750.	0	45	35	0	0	0	0	0	0	0	0	29	51	0	0	0	0	0	0	0	0	46	34	0	0	0	0	0	0	0	0	80	0	0	0	0	0	0	0	0
800.	0	[illegible]		0	0	0	0	0	0	0	0	54	26	0	0	0	0	0	0	0	0	68	12	0	0	0	0	0	0	0	0	80	0	0	0	0	0	0	0	0
850.	0	[illegible]		0	0	0	0	0	0	0	0	72	8	0	0	0	0	0	0	0	0	79	1	0	0	0	0	0	0	0	3	77	0	0	0	0	0	0	0	0
900.	0	[illegible]		0	0	0	0	0	0	0	0	80	0	0	0	0	0	0	0	0	0	80	0	0	0	0	0	0	0	0	14	66	0	0	0	0	0	0	0	0
950.	0	80	0	0	0	0	0	0	0	0	0	80	0	0	0	0	0	0	0	0	0	80	0	0	0	0	0	0	0	0	29	51	0	0	0	0	0	0	0	0
1000.	0	80	0	0	0	0	0	0	0	0	0	80	0	0	0	0	0	0	0	0	0	80	0	0	0	0	0	0	0	0	50	30	0	0	0	0	0	0	0	0
1050.	0	80	0	0	0	0	0	0	0	0	0	80	0	0	0	0	0	0	0	0	0	80	0	0	0	0	0	0	0	0	68	12	0	0	0	0	0	0	0	0
1100.	0	80	0	0	0	0	0	0	0	0	0	80	0	0	0	0	0	0	0	0	0	80	0	0	0	0	0	0	0	0	75	5	0	0	0	0	0	0	0	0
1150.	0	80	0	0	0	0	0	0	0	0	0	80	0	0	0	0	0	0	0	0	0	80	0	0	0	0	0	0	0	0	80	0	0	0	0	0	0	0	0	0
1200.	0	80	0	0	0	0	0	0	0	0	0	80	0	0	0	0	0	0	0	0	0	80	0	0	0	0	0	0	0	0	80	0	0	0	0	0	0	0	0	0
1250.	0	80	0	0	0	0	0	0	0	0	0	30	0	0	0	0	0	0	0	0	1	79	0	0	0	0	0	0	0	0	80	0	0	0	0	0	0	0	0	0
1300.	5	75	0	0	0	0	0	0	0	0	1	79	0	0	0	0	0	0	0	0	3	77	0	0	0	0	0	0	0	0	80	0	0	0	0	0	0	0	0	0
1350.	8	72	0	0	0	0	0	0	0	0	5	75	0	0	0	0	0	0	0	0	11	69	0	0	0	0	0	0	0	0	80	0	0	0	0	0	0	0	0	0
1400.	15	65	0	0	0	0	0	0	0	0	8	72	0	0	0	0	0	0	0	0	20	60	0	0	0	0	0	0	0	0	80	0	0	0	0	0	0	0	0	0
1450.	28	52	0	0	0	0	0	0	0	0	15	65	0	0	0	0	0	0	0	0	31	49	0	0	0	0	0	0	0	0	80	0	0	0	0	0	0	0	0	0
1500.	45	35	0	0	0	0	0	0	0	0	28	52	0	0	0	0	0	0	0	0	47	33	0	0	0	0	0	0	0	0	80	0	0	0	0	0	0	0	0	0
1550.	56	24	0	0	0	0	0	0	0	0	42	38	0	0	0	0	0	0	0	0	57	23	0	0	0	0	0	0	0	0	80	0	0	0	0	0	0	0	0	0
1600.	66	14	0	0	0	0	0	0	0	0	54	26	0	0	0	0	0	0	0	0	68	12	0	0	0	0	0	0	0	0	80	0	0	0	0	0	0	0	0	0
1650.	73	7	0	0	0	0	0	0	0	0	63	17	0	0	0	0	0	0	0	0	75	5	0	0	0	0	0	0	0	0	80	0	0	0	0	0	0	0	0	0
1700.	78	2	0	0	0	0	0	0	0	0	72	8	0	0	0	0	0	0	0	0	79	1	0	0	0	0	0	0	0	0	80	0	0	0	0	0	0	0	0	0
1750.	80	0	0	0	0	0	0	0	0	0	78	2	0	0	0	0	0	0	0	0	80	0	0	0	0	0	0	0	0	0	80	0	0	0	0	0	0	0	0	0
1800.	80	0	0	0	0	0	0	0	0	0	80	0	0	0	0	0	0	0	0	0	80	0	0	0	0	0	0	0	0	0	80	0	0	0	0	0	0	0	0	0
1850.	80	0	0	0	0	0	0	0	0	0	80	0	0	0	0	0	0	0	0	0	80	0	0	0	0	0	0	0	0	0	80	0	0	0	0	0	0	0	0	0
1900.	80	0	0	0	0	0	0	0	0	0	80	0	0	0	0	0	0	0	0	0	80	0	0	0	0	0	0	0	0	0	80	0	0	0	0	0	0	0	0	0
1950.	80	0	0	0	0	0	0	0	0	0	80	0	0	0	0	0	0	0	0	0	80	0	0	0	0	0	0	0	0	0	80	0	0	0	0	0	0	0	0	0
2000.	80	0	0	0	0	0	0	0	0	0	80	0	0	0	0	0	0	0	0	0	80	0	0	0	0	0	0	0	0	0	80	0	0	0	0	0	0	0	0	0

Figure 6.- Detection interval vs step failure level for 980°/hr summed parity residual detection threshold.

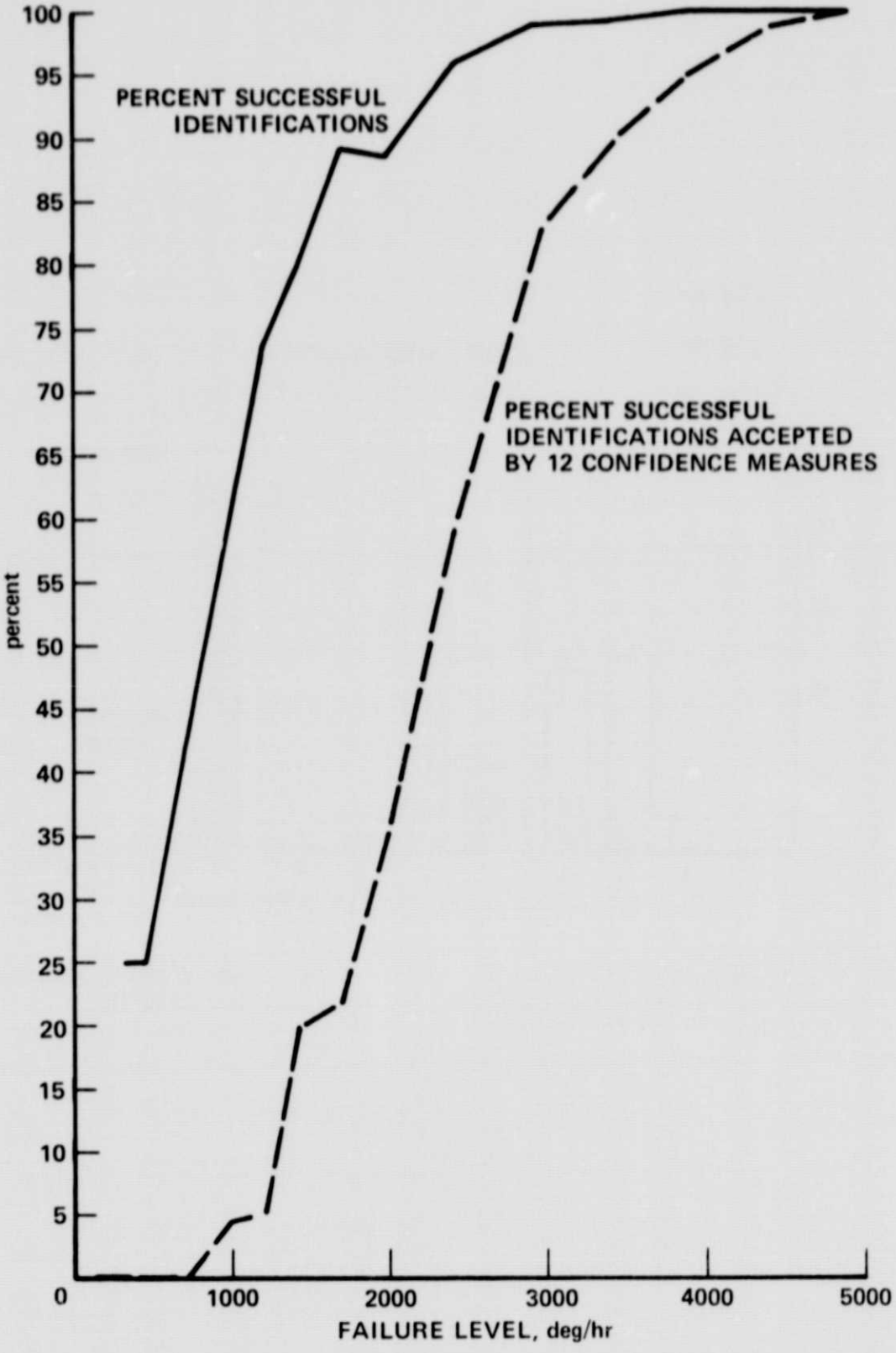

Figure 7.- Confidence measures rejection of successful identifications by tetrad FO-FS strategy (for fit interval 5 points and fit order 1) vs failure step level.

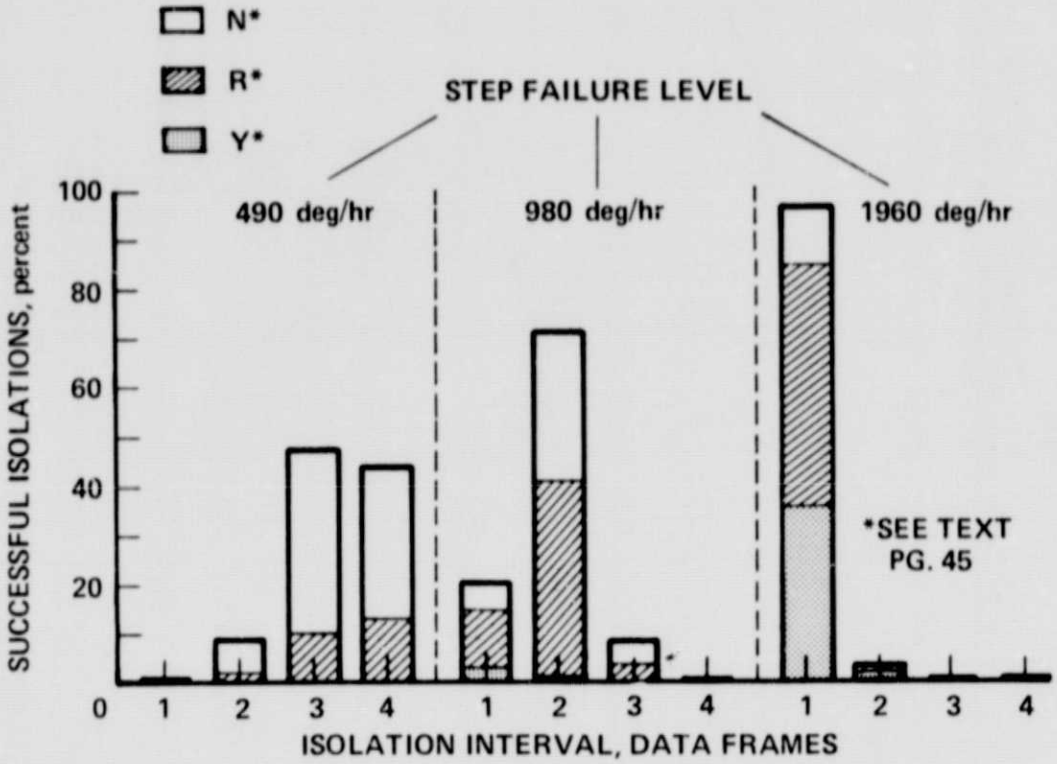

Figure 8.- Frames required to detect and isolate sensor failure (isolation interval) for step failures 490°/hr, 980°/hr, and 1960°/hr.

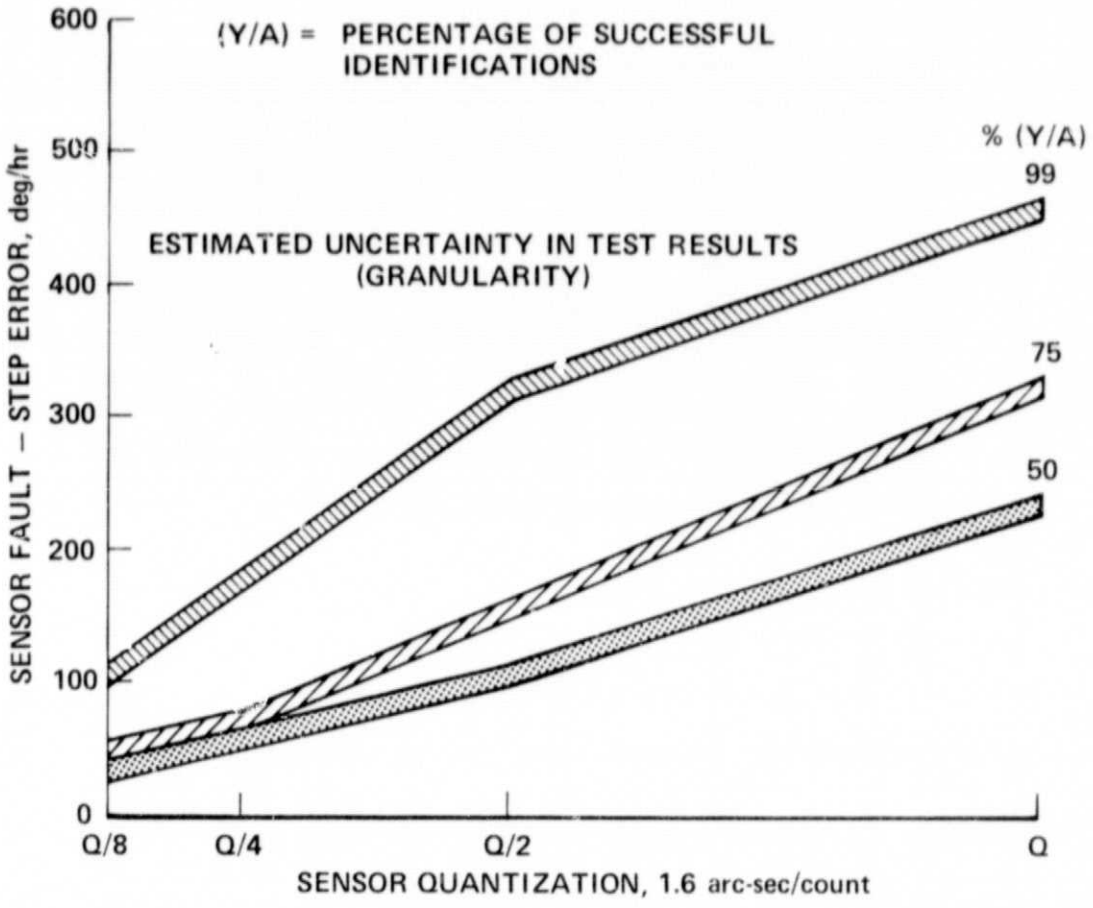

Figure 9.- Successful identification level vs sensor quantization (determined from noise-free simulated gyro data).

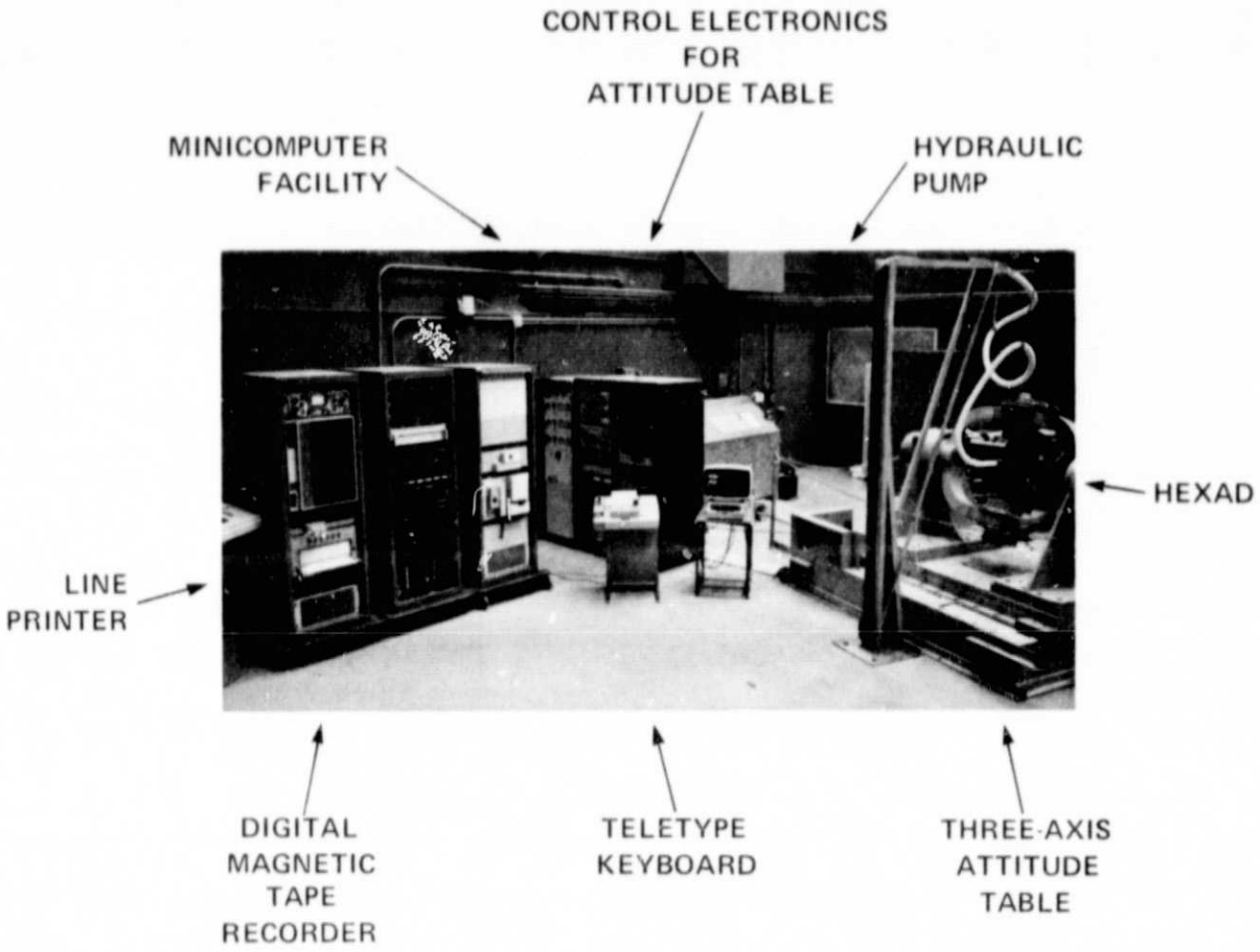

Figure 10.- Facility for testing strap-down inertial systems.

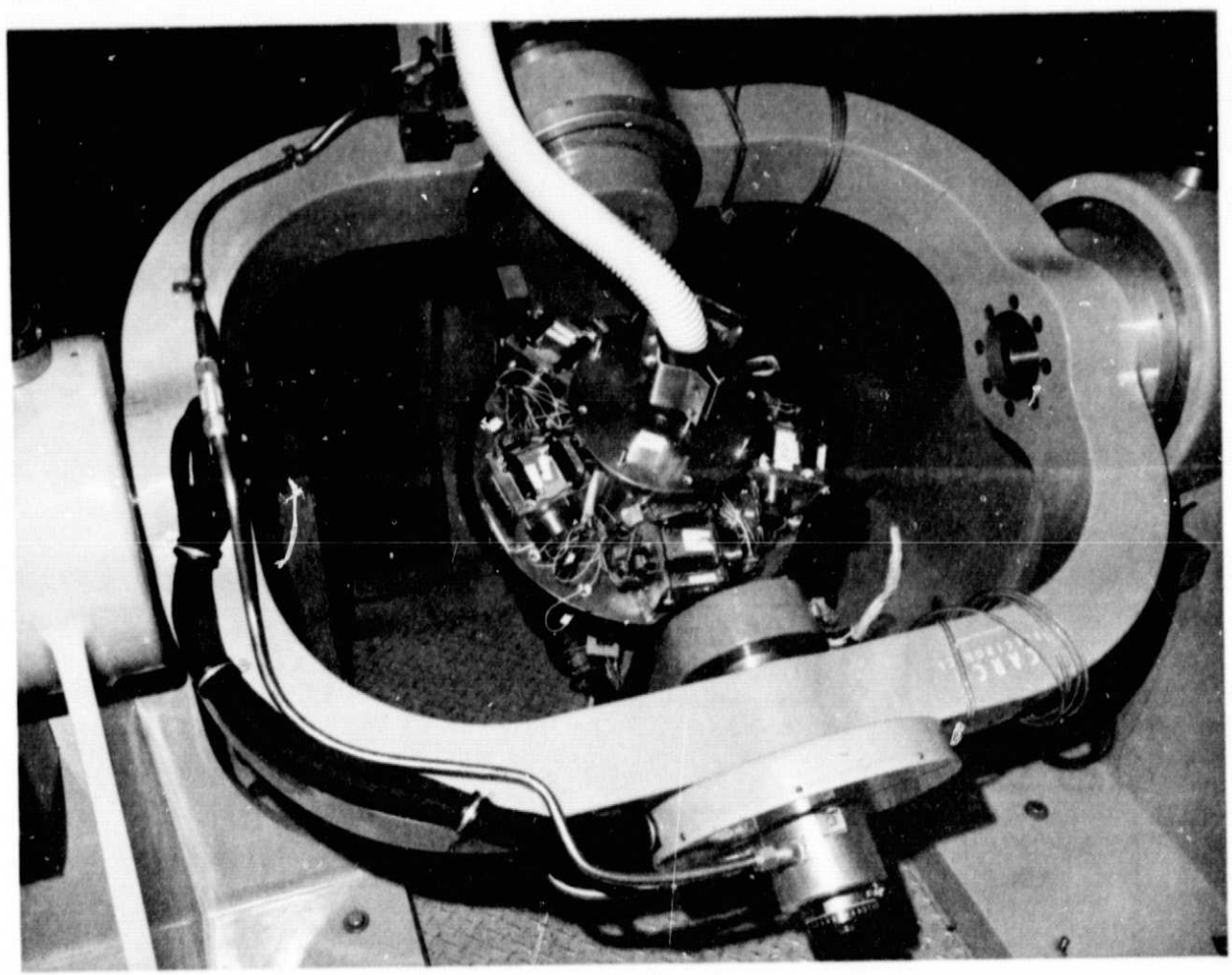

Figure 11.- Strap-down, variable angle, hexad inertial sensor assembly.

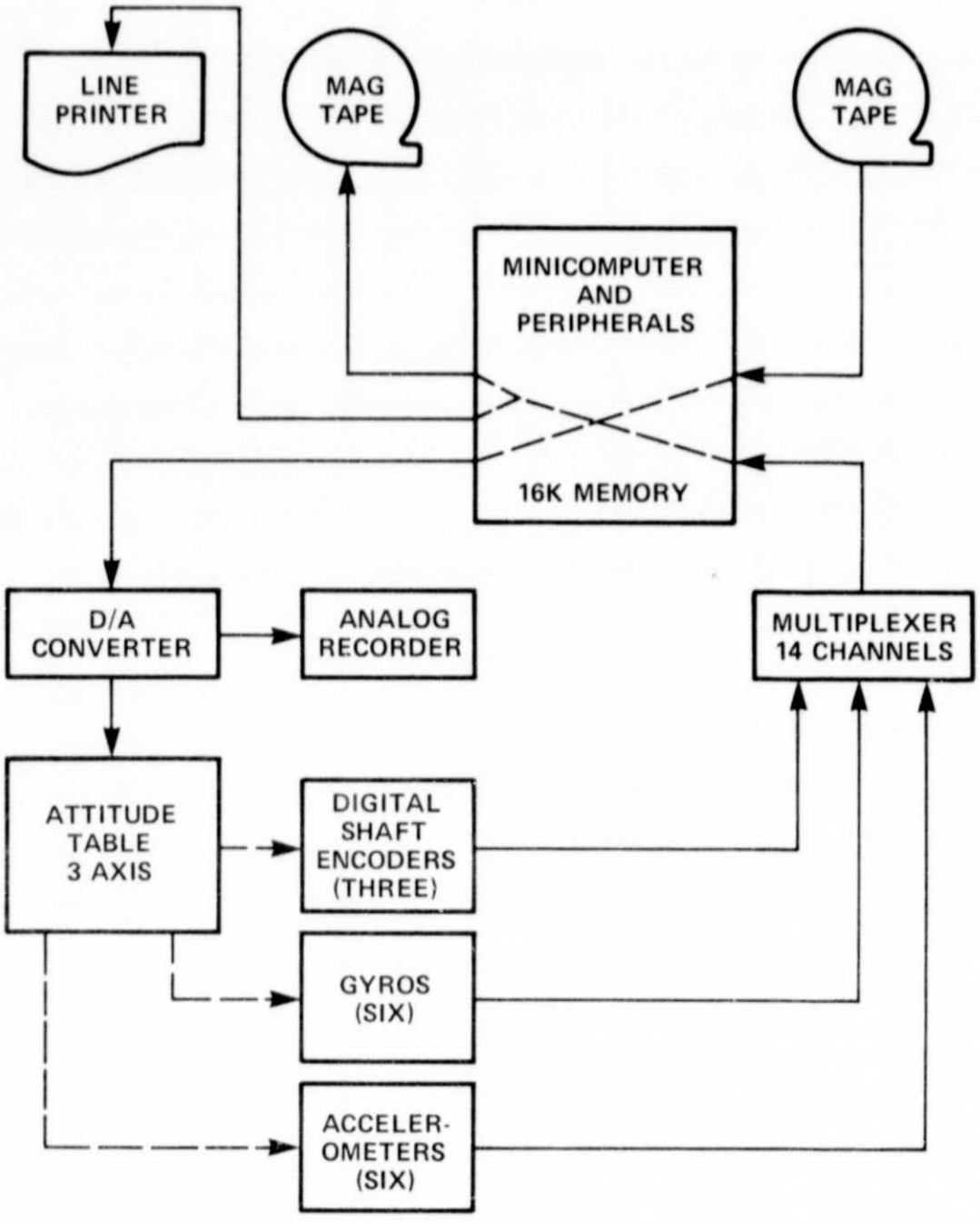

Figure 12.- Data acquisition system schematic.

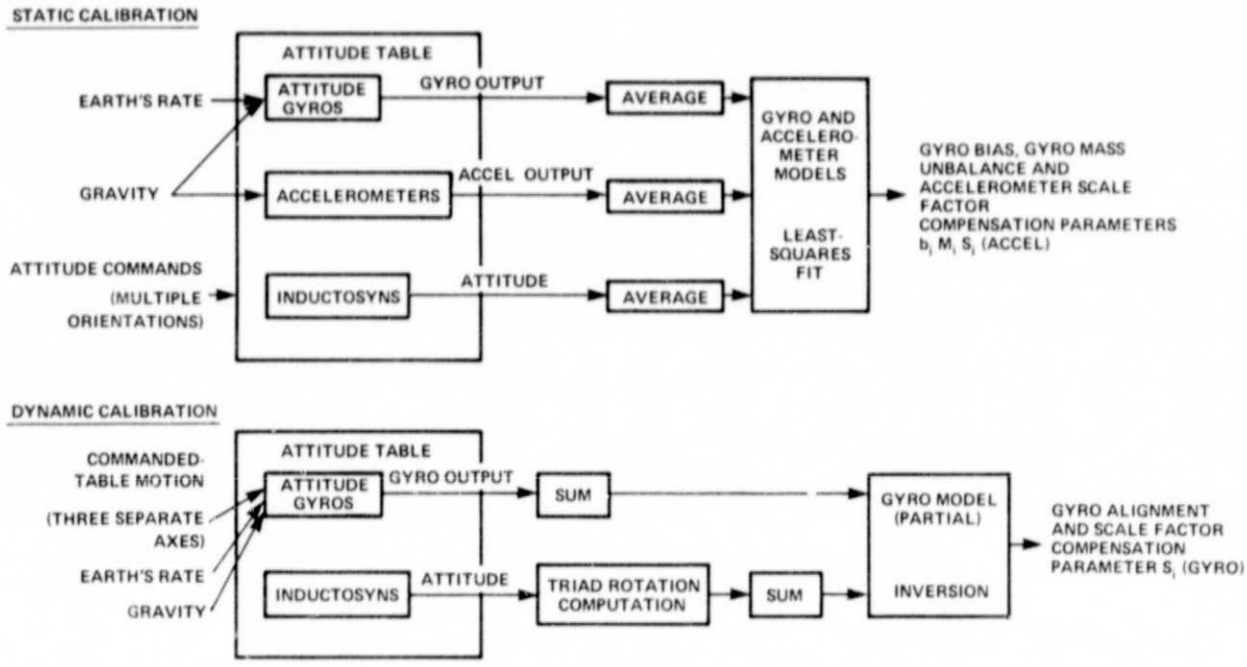

Figure 13.- Information flowgraph for static and dynamic calibration.

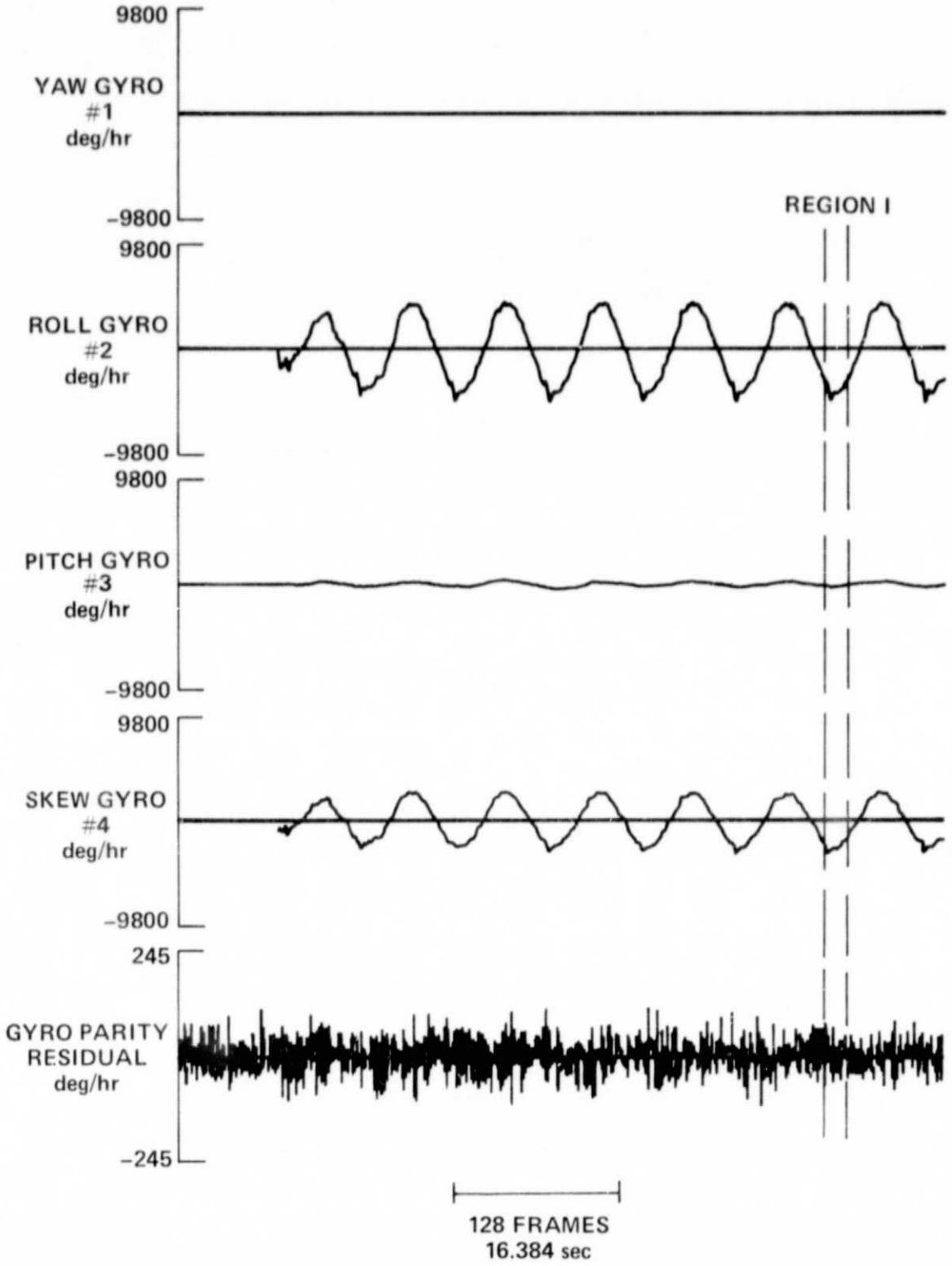

Figure 14.- Attitude gyro outputs and parity residual for 0.1-hz pitching motion.

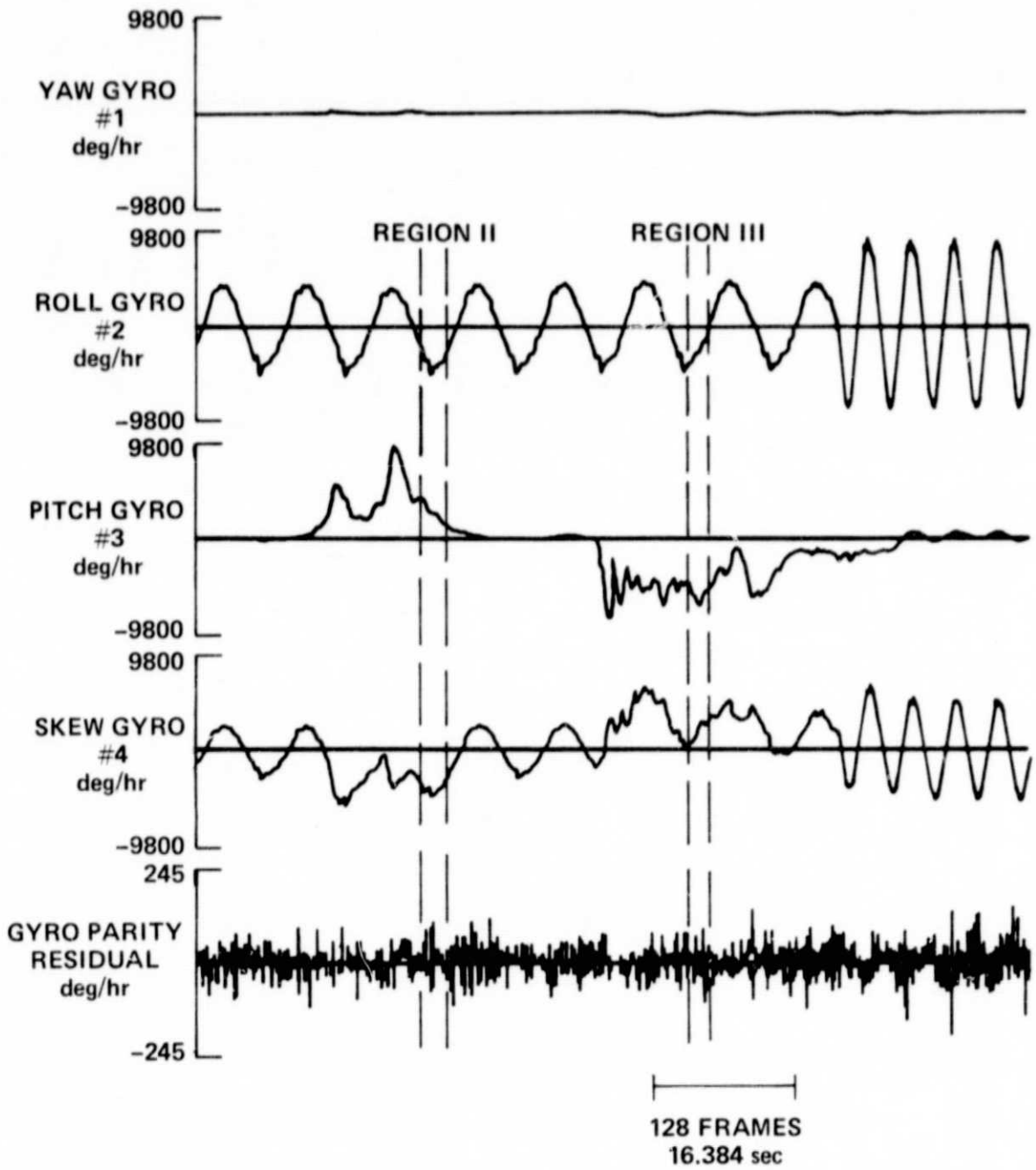

Figure 15.- Attitude gyro outputs and parity residual for 0.1-hz pitching and 0.03-hz rolling motion.

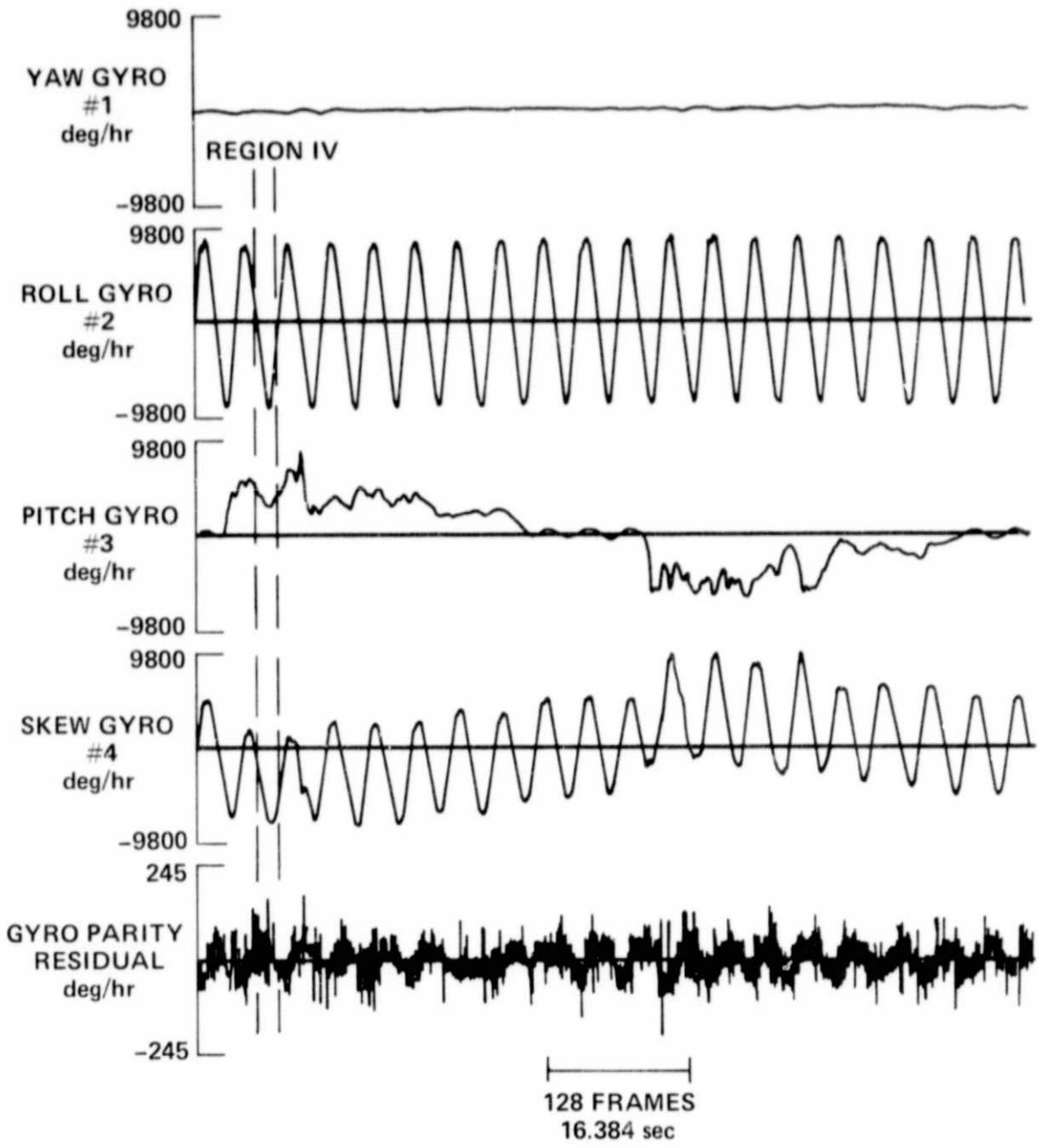

Figure 16.- Attitude gyro outputs and parity residual for 0.2-hz pitching motion.